



**HAL**  
open science

# Kinetics of precipitation of non-ideal solid-solutions in a liquid environment

Claudine Noguera, B. Fritz, A. Clement

► **To cite this version:**

Claudine Noguera, B. Fritz, A. Clement. Kinetics of precipitation of non-ideal solid-solutions in a liquid environment. *Chemical Geology*, 2016, 431, pp.20-35. 10.1016/j.chemgeo.2016.03.009 . hal-01297452

**HAL Id: hal-01297452**

**<https://hal.sorbonne-universite.fr/hal-01297452v1>**

Submitted on 4 Apr 2016

**HAL** is a multi-disciplinary open access archive for the deposit and dissemination of scientific research documents, whether they are published or not. The documents may come from teaching and research institutions in France or abroad, or from public or private research centers.

L'archive ouverte pluridisciplinaire **HAL**, est destinée au dépôt et à la diffusion de documents scientifiques de niveau recherche, publiés ou non, émanant des établissements d'enseignement et de recherche français ou étrangers, des laboratoires publics ou privés.

# Kinetics of precipitation of non-ideal solid-solutions in a liquid environment.

C. Noguera,<sup>1</sup> B. Fritz,<sup>2</sup> and A. Clément<sup>2</sup>

<sup>1</sup>*CNRS-Sorbonne Universités, UPMC Univ. Paris 06, UMR 7588, INSP, F-75005 Paris, France*

<sup>2</sup>*Université de Strasbourg/EOST, CNRS, Laboratoire d'Hydrologie et de Géochimie de Strasbourg, 1 rue Blessig, F-67084 Strasbourg Cedex, France*

(Dated: April 1, 2016)

We present a theoretical formalism which, for the first time, accounts for the nucleation, growth and/or redissolution of binary non-ideal solid-solutions, whether mineral or bimetallic, in solution. It yields the time evolution of all ion activities, together with the particle population characteristics: number, size and composition profile of particles as a function of time and of their time of nucleation. It is shown that depending on the Guggenheim parameter values which drive the non-ideality of the solid-solution, on the ratio of the solubility products of the end-members and on initial conditions, different scenarios of precipitation may take place, in which particles display composition profiles which may be smooth or discontinuous. An illustration of the characteristics of precipitation in the various scenarios is given, by simulations performed under some simplifying assumptions and qualitative predictions are made for the precipitation of some mineral solid solutions of geochemical interest. To our knowledge, this is the first time, in the fields of both geochemistry and metallic alloys, that these out-of-equilibrium precipitation processes of non-ideal solid-solutions are fully described.

Highlights:

- Theoretical and numerical model for out-of-equilibrium precipitation of non-ideal solid solutions in a liquid medium.
- For the first time, nucleation, growth and/or redissolution processes are fully described.
- Particle size distribution functions and composition profiles are obtained.
- The formalism applies to mineral  $A_{1-x}B_xC$  as well as bimetallic  $A_{1-x}B_x$  nanoparticle formation.
- Four scenarios are highlighted; predictions for the precipitation of mineral solid solutions of geochemical interest are made.

*Keywords:* nucleation and growth, non-ideal solid solutions, miscibility gap, clay minerals, bimetallic nanoparticles, alloy nanoparticles, core-shell nanoparticles, wet-chemical synthesis, kinetic simulation, Nanokin code.

PACS numbers:

## I. INTRODUCTION

In natural water-rock interaction systems on the Earth surface, primary minerals are often in a thermodynamic nonequilibrium state. This is the key-condition for the alteration which takes place in the water cycle, including both weathering processes near surface and hydrothermal alteration at depth. The resulting spontaneous dissolution of primary minerals leads to the formation of secondary minerals which are generally not defined compounds but often solid solution phases (SS), with compositions that adjust to the evolution of the chemical composition of the aqueous solution (AS). The most frequent example of this property is the formation of clay mineral phases in the alteration of rock-forming silicates (Millot, 1970; Meunier and Velde, 1989), but many oxides, carbonates, and sulfates also share this property (Drever, 1984; Geiger, 2001; Rhada and Navrotsky, 2013).

In another context, formation of bimetallic nanoparticles is often the aim of wet chemistry experiments in the laboratory, due to their interesting properties for plasmonics (Major et al., 2009), catalysis (Zhang et al.,

2011) or electrocatalysis (Peng and Yang, 2009) applications. Similarly to their mineral counterparts, these alloys may display an ideal SS behavior, or, alternatively, a tendency towards ordering or demixing (phase separation), depending upon the sign and strength of their mixing enthalpy of formation (Ferrando et al., 2008).

The equilibrium behavior of a SS in contact with an AS, whether ideal or non-ideal, is now well established (Lippmann, 1982; Glynn and Reardon, 1990), as reviewed by Ganguly (2001) or Prieto (2009). The relationship between the SS composition and the distribution of ions in the AS may be represented by the classical Lippmann's or Roozeboom's diagrams (Lippmann, 1980; Roozeboom, 1904). Recent theoretical studies of non-ideal mineral SSs at equilibrium mainly concern cements and concretes interacting with the AS, particularly in the field of nuclear waste storages and clay barriers (Börjesson et al., 1997; Walker et al., 2007) but carbonate SSs have also been considered (Kulik et al., 2010; Katsikopoulos et al., 2009).

As far as the kinetics of SS formation are concerned, experiments making use of counter-diffusion of reactants

through a porous medium (Prieto et al., 1997; Sánchez-Pastor et al., 2006) or in situ atomic force microscopy studies of the growth of SSs in a fluid cell (Pina et al., 2000; Putnis et al., 2002; Astilleros et al., 2003; Astilleros et al., 2006) have provided important information on growth mechanisms and particle composition for various mineral SSs.

Inclusion of kinetic effects in the modeling of a SS formation still remains a difficult task. In the water-rock interaction model KINDIS (Madé et al., 1994) and its extension for treating reaction and transport (Nourtier-Mazauric et al., 2005), kinetic dissolution and precipitation at equilibrium of ideal SSs were included but without considering nucleation and growth. In these works, a single SS was allowed to precipitate for a given set of end-members, corresponding to the least soluble phase or, equivalently, to the phase with the highest supersaturation. More recent approaches rely on empirical rate equations, not considering explicitly nucleation, size-dependent growth and nucleation (Shtukenberg et al., 2010, Brandt et al., 2015). The same was true in the coupled reaction and transport model by Lichtner and Carey (2006) who represented the SS by a discrete set of stoichiometric solids with fixed composition. On the other hand, atomistic Monte Carlo simulations of ideal SSs under constant supersaturation have specified how the distribution coefficients vary with the supersaturation at kink, step and terrace sites of the growing particles (Matsumoto and Kitamura, 2001; Matsumoto et al., 2005). Only in the work of Pina and Putnis (2002) did a generalized expression for the nucleation rate appear, and the composition of the critical nucleus was determined from the maximum of the nucleation frequency. However, growth and feed-back effects were not included in this work.

To our knowledge, only in our previous works (Noguera et al., 2010; Noguera et al., 2012), were the full dynamics of a SS formation fully accounted for, with the inclusion of nucleation processes, size dependent growth, particle population and out-of-equilibrium composition of the critical nuclei and deposited layers during growth. This has led to the creation of a second version of the NANOKIN code (Noguera et al., 2010), which previously could only account for the kinetics of formation of minerals with fixed composition (Fritz et al., 2009). However, this second version was restricted to ideal binary SSs.

It is our goal, in the present work, to propose a theoretical description of nucleation and growth of *non-ideal* binary SSs. As will appear clearly in the following, it does not consist in merely introducing activity coefficients in the nucleation and growth equations. Depending on the strength of the enthalpy of mixing, which will be represented by a Guggenheim expansion restricted to two terms (sub-regular SS), and depending on the composition of the AS, several scenarios may take place in which the composition profiles of the formed particles and the precipitation dynamics are distinctly different. Each of these scenarios will be exemplified by a numerical simu-

lation, under some simplifying assumptions and predictions will be made for various mineral SSs of geochemical interest to assess which scenario applies to each of them.

The formalism primarily aims at describing SSs of the  $A_{1-x}B_xC$  type, relevant e.g. to mineral SSs with homovalent substitution, like  $(Ba,Sr)CO_3$ . However the generalization to SSs of the  $A_{1-x}B_x$  type, such as bimetallic SSs, is straightforward because it only requires skipping the C activities. In that way, our work can also be useful in the field of metallic alloys in which, to our knowledge, only thermodynamic aspects of the formation of bimetallic nanoparticles in wet chemistry experiments have been considered. We will use the generic term "aqueous" solution to refer to the solution in which precipitation takes place, whether it contains water or not.

The paper is organized as follows. In section II, we introduce thermodynamic concepts which are required for describing binary non-ideal (sub-regular) SSs in contact with an AS. We propose a new representation of the stoichiometric saturation condition, distinct from the Roozeboom diagram. It is more compact than the latter and turns out to be extremely useful in understanding the scenarios of precipitation of strongly non-ideal SSs. In section III, IV and V we present the theoretical background and master equations for nucleation, growth and feed-back effects on the chemical composition of the AS, respectively. Then, in Section VI, we discuss the characteristics of the precipitation process as a function of the degree of non-ideality of the SS and the initial conditions. We highlight four possible scenarios of precipitation and we devise a diagram of their occurrence as a function of the solid and AS characteristics. Finally, we illustrate the characteristics of precipitation in the various scenarios, by simulations performed within some simplifying assumptions, and we make qualitative predictions of the precipitation characteristics of SSs of geochemical interest (Section VII), before concluding. The text is complemented by five appendices in which most of the formal equations are derived.

## II. THERMODYNAMIC CONCEPTS

In this section we first recall some useful concepts relevant for a SS in contact with an AS of given composition. This will allow us to introduce quantities, such as the stoichiometric solubility product, the stoichiometric saturation state of the AS with respect to the SS, and the concept of stoichiometric saturation. Then we will discuss in detail how the latter depends on the non-ideality characteristics of the SS, which will be a useful step before addressing out-of-equilibrium processes.

We consider a SS of composition  $A_{1-x}B_xC$  ( $0 < x < 1$ ), with AC and BC its end-members. In the following, A, B and C will represent the relevant aqueous species in the AS and [A], [B] and [C] their activities, respectively. The solubility products of the end-members, denoted

164  $K_{AC}$  and  $K_{BC}$ , are functions of the standard changes  
165 in Gibbs free energy,  $\Delta G_{AC}$  and  $\Delta G_{BC}$ , for dissolution:206

$$\begin{aligned} K_{AC} &= \exp(-\Delta G_{AC}/RT) \\ K_{BC} &= \exp(-\Delta G_{BC}/RT) \end{aligned} \quad (1)$$

166 in which  $R$  is the gas constant and  $T$  the temperature.

167 Considering the SS as a single component stoichiomet-  
168 ric solid, the change of Gibbs free energy  $\Delta G(x)$  during  
169 the dissolution of one mole of composition  $x$  may be writ-  
170 ten as:

$$\begin{aligned} \Delta G(x) &= (1-x)\Delta G_{AC} + x\Delta G_{BC} + \Delta G_M^E(x) \\ &\quad -RT(x \ln x + (1-x) \ln(1-x)) \end{aligned} \quad (2)$$

171 The sum  $(1-x)\Delta G_{AC} + x\Delta G_{BC}$  represents the change  
172 of Gibbs free energy for a mechanical mixture of AC and  
173 BC. It is complemented by the ideal entropy of mix-  
174 ing (on the second line), assuming full disorder of the  
175 A and B species in the SS.  $\Delta G_M^E(x)$  is the excess free  
176 energy of mixing, which includes the excess entropy of  
177 mixing  $\Delta S_M^E(x)$  and the enthalpy of mixing  $\Delta H_M(x)$ :  
178  $\Delta G_M^E(x) = \Delta H_M(x) - T\Delta S_M^E(x)$ . We will neglect  
179  $\Delta S_M^E(x)$  which may originate from non-configurational  
180 entropy (Benisek and Dachs, 2012) or deviations from  
181 perfect randomness. As regards  $\Delta H_M(x)$ , whose varia-  
182 tions with the SS composition are usually represented by  
183 the Guggenheim expansion (Guggenheim, 1937), we will  
184 only keep its first two terms, and thus restrict ourselves  
185 to sub-regular SS:

$$\Delta H_M(x) = -RTx(1-x)[A_0 + A_1(2x-1)] \quad (3)$$

186 The two dimensionless parameters  $A_0$  and  $A_1$  charac-  
187 terize the non-ideality of the SS.  $A_0$  may be related to  
188 first neighbor pairwise interactions. Its sign drives the  
189 tendency to ordering (if negative) or to unmixing (if pos-  
190 itive). When  $A_0$  exceeds some critical value, the SS pos-  
191 sesses a miscibility gap, which means a range of compo-  
192 sitions in which phase separation takes place. The  $A_1$   
193 coefficient introduces an asymmetry of  $\Delta G_M^E(x)$  about  
194  $x = 1/2$ .

195 The stoichiometric solubility product of the SS:  
196  $K(x) = \exp(-\Delta G(x)/RT)$  is equal to:

$$K(x) = K_{AC}^{1-x} K_{BC}^x (1-x)^{1-x} x^x e^{x(1-x)[A_0 + A_1(2x-1)]} \quad (4)$$

197 One can deduce the stoichiometric saturation state  $I(x)$   
198 of the AS with respect to a SS of composition  $x$  (some-  
199 times called  $\beta(x)$  (Prieto et al., 1993)), equal to the ratio  
200 between the ionic activity product  $Q(x) = [A]^{1-x}[B]^x[C]$   
201 and  $K(x)$ :

$$I(x) = \left[ \frac{I_{AC}}{(1-x)} \right]^{1-x} \left[ \frac{I_{BC}}{x} \right]^x e^{-x(1-x)[A_0 + A_1(2x-1)]} \quad (5)$$

202 In this expression,  $I_{AC}$  and  $I_{BC}$  are the saturation states  
203 of the AS with respect to the pure end-members AC and  
204 BC, respectively:

$$I_{AC} = \frac{[A][C]}{K_{AC}} \quad ; \quad I_{BC} = \frac{[B][C]}{K_{BC}} \quad (6)$$

$I(x)$  can also be written in terms of the activity coeffi-  
cients  $\lambda_{AC}$  and  $\lambda_{BC}$  of the end-members:

$$I(x) = \left[ \frac{I_{AC}}{(1-x)\lambda_{AC}(x)} \right]^{1-x} \left[ \frac{I_{BC}}{x\lambda_{BC}(x)} \right]^x \quad (7)$$

The coefficients  $\lambda_{AC}$  and  $\lambda_{BC}$  depend on  $x$  and, for a  
sub-regular SS, are equal to (Glynn, 1991):

$$\begin{aligned} \lambda_{AC}(x) &= e^{x^2[A_0 + A_1(4x-3)]} \\ \lambda_{BC}(x) &= e^{(1-x)^2[A_0 + A_1(4x-1)]} \end{aligned} \quad (8)$$

Thermodynamic equilibrium between the SS and the  
AS is reached when simultaneously  $I(x) = 1$  (equivalent  
to  $\Delta G(x) = -RT \ln Q(x)$ ), and  $I(x)$  is maximum with  
respect to  $x$ . These two conditions determine the compo-  
sition  $x_0$  of the SS and that of the AS (through the  
values of  $I_{AC}$  and  $I_{BC}$ ) at thermodynamic equilibrium.  
They can be recast under the standard form:

$$\begin{aligned} I_{AC} &= (1-x_0)\lambda_{AC}(x_0) \\ I_{BC} &= x_0\lambda_{BC}(x_0) \end{aligned} \quad (9)$$

In the following, we will focus on the characteristics  
of the *stoichiometric saturation state*, obtained from the  
single condition that  $I(x)$  is maximum with respect to  
 $x$ . Indeed, the goal of our work is to describe the *ki-*  
*netics* of precipitation and not the thermodynamic equi-  
librium between an AS and a SS, which is only found  
at infinite time of the precipitation process. Using the  
stoichiometric saturation amounts to considering the SS  
with respect to which the AS is the most supersaturated  
(Prieto, 2009). Its composition  $x_{st}$  is the solution of the  
implicit equation (Appendix A):

$$\frac{I_{AC}}{\lambda_{AC}(x_{st})(1-x_{st})} = \frac{I_{BC}}{\lambda_{BC}(x_{st})x_{st}} \quad (10)$$

Such a relationship is often graphically represented in a  
Roozeboom plot  $(x_{st}, [B]/([A]+[B]))$  (Mullin, 1993). The  
discussion which follows, based on Equation 10, paves  
the route to understanding the composition of the critical  
nuclei which will be the subject of the following section.

As shown in Appendix A, Eq. 10 may have one or  
three roots, depending on the values of  $A_0$ ,  $A_1$ , and on  
the composition of the AS. The latter enters in a compact  
way through the ratio  $W$ , which is equal to:

$$W = \frac{I_{BC}}{I_{AC}} = \frac{[B]K_{AC}}{[A]K_{BC}} \quad (11)$$

When Eq. 10 has a single root,  $x_{st}$  varies smoothly as a  
function of  $W$ . When there are three roots, two corre-  
spond to maxima of  $I(x)$  (i.e. minima of  $-\ln I(x)$ ) and  
one to a minimum (Figure 11 in Appendix A). The com-  
position  $x_{st}$  is equal to the root associated with the low-  
est value of  $-\ln I(x)$ . In Figure 1 are represented typical  
variations of the three roots of Eq. 10 as a function of  $W$   
and of the corresponding three values of  $-\ln(I(x)/I_{AC})$

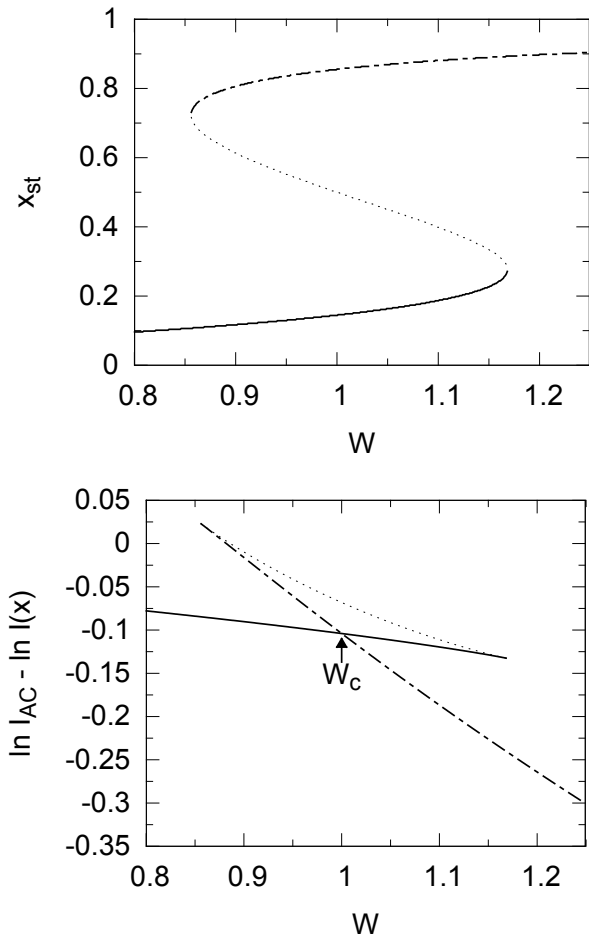


FIG. 1: Top panel: the three roots of Eq. 10, as a function of  $W = I_{BC}/I_{AC}$ , when  $A_0 = 2.5$  and  $A_1 = 0$ . The full and dashed-dotted curves display the variations of the minima of  $-\ln I(x)$  while the dotted one is associated with the maximum of this function. Bottom panel, corresponding values of  $\ln I_{AC} - \ln I(x)$ . The composition  $x_{st}$  of the SS at stoichiometric saturation corresponds to the lowest value of this function. The crossing of the curves at  $W_c$  is associated to a discontinuity of  $x_{st}$ .

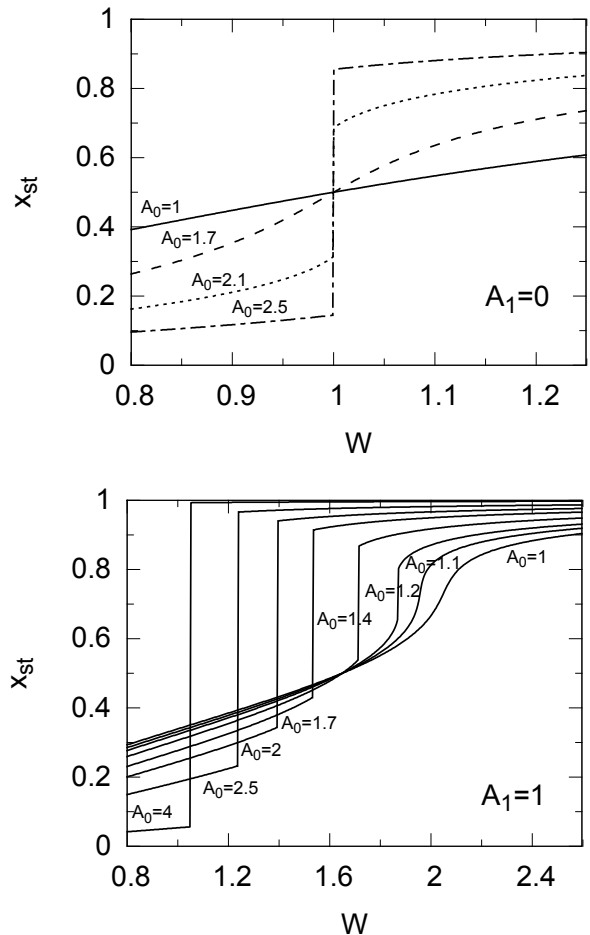


FIG. 2: Composition  $x_{st}$  of a SS at stoichiometric saturation with an AS whose composition is characterized by  $W = I_{BC}/I_{AC}$ , for various values of  $A_0$  when  $A_1 = 0$  (top panel) or  $A_1 = 1$  (bottom panel).

in the case of a strongly non-ideal SS. Because the lat-  
 244 ter cross each other, a discontinuity in  $x_{st}$  between two  
 245 values  $x_1$  and  $x_2$  takes place for some AS composition  
 246 characterized by  $W = W_c$ , at which the two phases of  
 247 composition  $x_1$  and  $x_2$  have the same Gibbs free energy  
 248 per mole. When  $W = W_c$ , the solid phase may become  
 249 spatially inhomogeneous and separate into two phases of  
 250 compositions  $x_1$  and  $x_2$ .

Figure 2 shows the variations of  $x_{st}$  as a function of  $W$   
 253 for several values of  $A_0$  and  $A_1$ . In the case of regular  
 254 SSs ( $A_1 = 0$ ),  $x_{st}$  varies smoothly (single root in Eq.  
 255 10) as long as  $A_0$  remains smaller than 2.  $x_{st}$  is less  
 256 than 0.5 (which means that the SS is richer in A ions  
 257 than in B ions) whenever  $W < 1$  and larger than 0.5 in  
 258 the opposite case. When  $A_0$  exceeds 2, a discontinuity  
 259 occurs at  $W_c = 1$ , whose height increases with  $A_0$  (e.g.  
 260  $x_2 - x_1 \approx 0.4$  for  $A_0 = 2.1$  and 0.7 for  $A_0 = 2.5$ ). The

symmetry of the miscibility gap about  $x_{st} = 1/2$  is to be  
 linked to the shape of the Gibbs free energy of mixing.

In sub-regular SSs ( $A_1 \neq 0$ ), the transition between  
 smooth and discontinuous variations of  $x_{st}$  occurs at  
 smaller values of  $A_0$  and the discontinuity (when it ex-  
 263 ists) takes place at varying values of  $W_c$ .  $x_1$  and  $x_2$  are  
 264 no longer symmetric about 0.5.

The dependence of  $W_c$  on  $A_0$  is represented in Figure  
 3 (top panel).  $W_c$  decreases (resp. increases) asymptotically  
 towards  $W_c = 1$ , as  $A_0$  becomes larger if  $A_1 > 0$   
 (resp.  $A_1 < 0$ ). On each curve, there exists a minimum  
 value of  $A_0$  below which the discontinuity disappears and  
 $x_{st}$  recovers a smooth variation as a function of the AS  
 composition. The range of parameters  $\{A_0, A_1\}$  for which  
 $x_{st}$  has no discontinuity lies inside the region delineated  
 by the two curves drawn in Figure 3 (bottom panel).

Compared to the Roozeboom plot, the representation  
 of  $x_{st}$  as a function of  $W = ([B]K_{AC})/([A]K_{BC})$  that  
 we propose presents several advantages. First it acknowl-  
 edges the fact that, at constant values of the Guggenheim

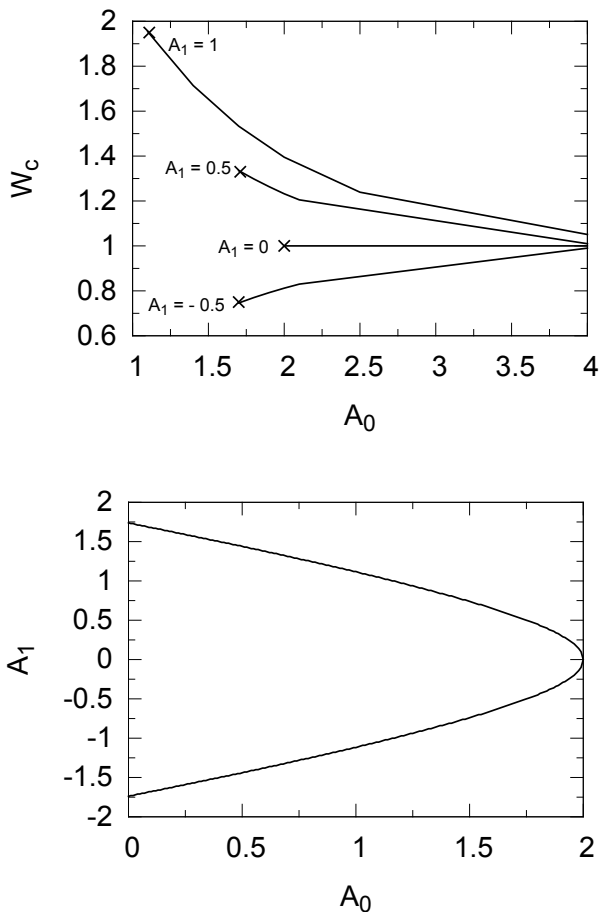


FIG. 3: Top: position  $W_c$  of the  $x_{st}$  discontinuity as a function of  $A_0$  for  $A_1=1, 0.5, 0$ , and  $-0.5$ . At constant  $A_1$ , the crosses mark the critical  $A_0$  value above which a discontinuity starts taking place. This critical value is represented in the bottom panel as a function of  $A_1$ . In the region between the two lines, Eq. 10 has a single root whatever  $W$ , which means that  $x_{st}$  varies smoothly as a function of the composition of the AS.

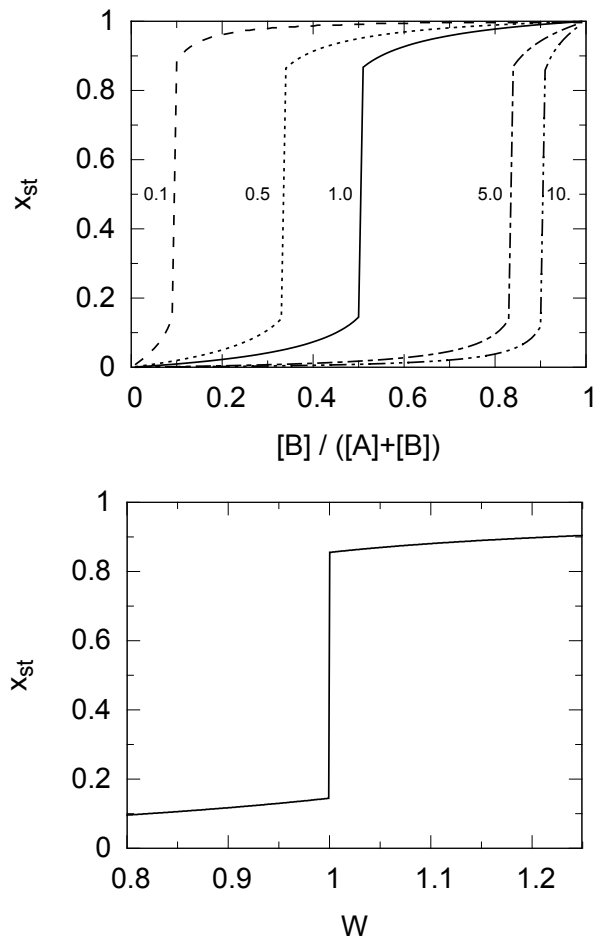


FIG. 4: Two representations of the relationship between the SS composition  $x_{st}$  and the AS composition. Top: Roozeboom plot as a function of  $[B]/([A] + [B])$  for various values of  $K_{BC}/K_{AC}$ . Bottom: Representation as a function of  $W = ([B]K_{AC})/([A]K_{BC})$ . In both case the SS is characterized by Guggenheim parameters  $A_0 = 2.5$  and  $A_1 = 0$ .

### III. NUCLEATION

In this section and the two following ones, we extend the formalism of nucleation and growth previously established for the precipitation of minerals with fixed composition (Noguera et al., 2006a,b) and ideal SSs (Noguera et al., 2010) to the formation of non-ideal SSs. Nucleation is treated within the framework of the classical theory of nucleation, in its continuum limit (Markov, 1995; Adamson, 1960). It is described in the following for homogeneous nucleation of spherical particles. The extension to heterogeneous nucleation (i.e. nucleation of particles on foreign solids) and non-spherical particle shapes is given in Appendix B. Moreover, we send the more complex treatment of precipitation of SSs whose surface energy depends on composition to Appendix C.

Under these conditions (homogeneous nucleation, spherical particles and constant surface energy), the

parameters,  $x_{st}$  is uniquely defined by the value of  $W$ , and not separately by the ratios  $[B]/[A]$  and  $K_{BC}/K_{AC}$  as in the Roozeboom representation. The latter, for which one plot is needed for each value of  $K_{BC}/K_{AC}$ , is convenient when one considers a specific system. At variance, the representation of  $x_{st}$  as a function of  $W$  is unique whatever the value of  $K_{BC}/K_{AC}$  (Figure 4). It will help highlight the generic behavior of sub-regular SSs during precipitation, which is the goal of our work. As will be shown in the next sections, a representation of the same type will be extremely useful to characterize the composition of the critical nuclei and layers deposited during growth, and to discriminate the various scenarios of precipitation.

change in Gibbs free energy  $\Delta G(n, x)$  in the formation of a nucleus containing  $n$  formula units of composition  $x$  is the sum of two terms ( $k_B$  the Boltzmann constant):

$$\Delta G(n, x) = -nk_B T \ln I(x) + n^{2/3} v(x)^{2/3} X \sigma \quad (12)$$

The first (bulk-like) term  $-nk_B T \ln I(x)$ , with  $I(x)$  the stoichiometric saturation state given by Eq. 7, represents the gain (if  $I(x) > 1$ ) of Gibbs free energy when ions from the AS condense into a solid phase. The second term  $E_s = n^{2/3} v(x)^{2/3} X \sigma$  is the total surface energy of the nucleus. In this expression,  $v(x)$  is the volume of a formula unit of composition  $x$ , that will be assumed to vary linearly between its end-member values (no excess molar volume):  $v(x) = (1-x)v_{AC} + xv_{BC}$ . The geometric factor  $X$  is equal to  $X = (36\pi)^{1/3}$  for spherical particles and  $\sigma$  is the surface energy per unit area.

When  $I(x) > 1$ ,  $\Delta G(n, x)$  displays a maximum as a function of  $n$ , which defines the characteristics of the critical nucleus: its size  $n_m(x)$  and the barrier to be overcome for its nucleation  $\Delta G_m(x) = \Delta G(n_m(x), x)$ :

$$n_m(x) = \frac{2u(x)}{\ln^3 I(x)} \quad \text{with } u(x) = \frac{4X^3 \sigma^3 v(x)^2}{27(k_B T)^3} \quad (13)$$

and :

$$\frac{\Delta G_m(x)}{k_B T} = \frac{u(x)}{\ln^2 I(x)} \quad (14)$$

Assuming that the flow of nuclei through size and composition space is confined to a path through this point only (Reiss and Shugard, 1976), the composition of the critical nuclei is determined by the condition that the nucleation frequency  $F(x)$  is maximum with respect to  $x$ .  $F(x)$  depends exponentially on the nucleation barrier  $\Delta G_m(x)$ :

$$F(x) = F_0 \exp\{-\Delta G_m(x)/k_B T\} \quad (15)$$

There have been attempts to theoretically estimate the prefactor  $F_0$  for specific systems. However, in most cases, it has resulted in huge (several orders of magnitude) discrepancies with measured values, even in the case of minerals of fixed composition. For this reason, we will assume it to be a constant, with a value that must be empirically determined. The maximum nucleation rate is thus obtained when  $\Delta G_m(x)$  is minimum with respect to  $x$ , in which case the critical nuclei correspond to a saddle point in the  $\Delta G(n, x)$  energy surface.

Taking these expressions into consideration, after some algebra (Appendix D), the minimization of the nucleation barrier yields the critical nucleus composition  $x^*$ , solution of the implicit equation:

$$\left( \frac{I_{AC}}{(1-x^*)\lambda_{AC}(x^*)} \right)^{v_{BC}} = \left( \frac{I_{BC}}{x^*\lambda_{BC}(x^*)} \right)^{v_{AC}} \quad (16)$$

For ideal SSs, Eq. 16 has a single root. For regular or sub-regular SSs, there may be one or three roots and one

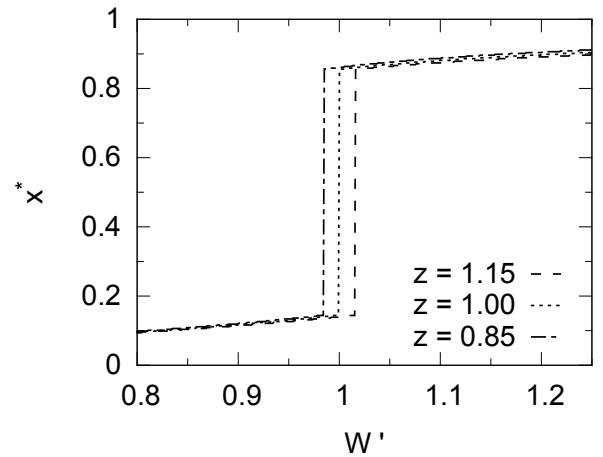


FIG. 5: Composition of the critical nuclei  $x^*$ , as a function of the ratio  $W' = I_{BC}/I_{AC}^z$ , for several values of  $z = v_{BC}/v_{AC}$ . All curves have been drawn for  $A_0 = 2.5$  and  $A_1 = 0$ . When  $z = 1$ ,  $x^* = x_{st}$ .

must determine the one which minimizes the nucleation barrier. To make a link with the previous section, one notes that, except for the exponents  $v_{AC}$  and  $v_{BC}$ , Eq. 16 strongly resembles Eq. 10, and, indeed, finding its solution(s) amounts to minimizing  $-\ln I(x)/v(x)$ . When  $v(x)$  does not depend on  $x$ , the composition  $x^*$  of the critical nucleus is thus equal to  $x_{st}$ , determined previously. When  $v$  varies with composition, the minimization of  $-\ln I(x)/v(x)$  is mathematically more involved (Appendix D). The solutions can be shown to be functions of  $A_0$ ,  $A_1$ ,  $z = v_{BC}/v_{AC}$  (parameter related to the end-member structures), and of the ratio:

$$W' = \frac{I_{BC}}{I_{AC}^z} \quad (17)$$

function of the composition of the AS. Depending upon whether the Guggenheim parameter values are located outside or within the region of the miscibility gap,  $x^*$  varies smoothly as a function of the AS composition or displays a discontinuity at a value  $W'_c$  function of  $A_0$ ,  $A_1$  and  $z$ . Usually  $z$  does not differ much from 1, especially for isomorphic end-members, because otherwise there would be no possibility to form an actual SS. As a result, in all cases, the composition  $x^*$  of the critical nucleus remains very close to  $x_{st}$ . Figure 5, for example, shows how  $x^*$  varies with  $W'$  for three values of  $z$ , in the case of a strongly non-ideal regular SS with  $A_0 = 2.5$ . The curve associated with  $z = 1$  represents the variations of  $x_{st}$ .  $W'_c$  varies by  $\pm 1.6\%$  when  $z = 1 \pm 0.15$ . The  $\{A_0, A_1\}$  range, in which a discontinuity of  $x^*$  occurs, nearly exactly coincides with that for  $x_{st}$  (Figure 3 bottom panel) within a precision of 0.001 on the limiting values of  $A_0$  and  $A_1$ .

Nucleation may start as soon as  $I(x^*) > 1$ . However, it becomes efficient (more than one nucleus per second and liter of solution), only if  $I(x^*)$  exceeds a critical value

388  $I_c(x^*)$  defined by:

$$\ln I_c(x^*) = \sqrt{\frac{u(x^*)}{\ln F_0}} \quad (18)$$

389 All quantities related to a given critical nucleus:  $x^*$ ,  
390  $n^* = n_m(x^*)$ ,  $\Delta G^* = \Delta G_m(x^*)$  and  $F(x^*)$ , depend on  
391 the time  $t_1$  at which nucleation occurs. This time depen-  
392 dence comes from the instantaneous values of the satu-  
393 ration states  $I_{AC}(t_1)$  and  $I_{BC}(t_1)$  of the AS with respect  
394 to the pure SS end-members, entering Eq. 16 which de-  
395 termines  $x^*(t_1)$ .

#### IV. GROWTH

397 Growth involves the condensation of ions from the AS  
398 on the surface of the particles. A growth law which cor-  
399 rectly describes such processes has to be size-dependent,  
400 but its expression depends upon the rate limiting pro-  
401 cess: diffusion in the liquid or the gaseous phase, contin-  
402 uous interfacial effects, and two-dimensional nucleation  
403 on flat faces or spiral growth (Burton et al., 1951; Baron-  
404 net, 1982; Parbhakar et al., 1995). In the following, we  
405 will restrict ourselves to a continuous growth mechanism,  
406 limited by the incorporation of growth units at the sur-  
407 face of a rough nucleus (Markov, 1995; Pina et al., 2000).  
408 Furthermore, we will define an average rate of incorpora-  
409 tion, so that the particle keeps the same shape as the  
410 critical nucleus (Wulff or Wulff-Kaishev shape) during its  
411 growth. Actually, the particle size may increase or de-  
412 crease according to whether it is larger or smaller than  
413 the instantaneous size of the critical nuclei. This is the  
414 Ostwald ripening process (Ostwald, 1900; Lifschitz and  
415 Slyozov, 1961). We will consider the two cases of positive  
416 growth or redissolution (negative growth) separately.

##### A. Positive growth

418 The energetic cost to increase the dimensions of a par-  
419 ticle may be related to its change of volume  $\delta V$  and its  
420 change of total surface energy  $\delta E_s$ :

$$\delta \Delta G(x) = -\frac{\delta V}{v(x)} k_B T \ln I(x) + \delta E_s \quad (19)$$

421 In the following, we will make the assumption of local  
422 equilibrium at the particle-solution interface. It amounts  
423 to considering that short-range transport across the in-  
424 terface is rapid enough to equilibrate the ions in the liquid  
425 and solid layers in contact. It is valid provided that the  
426 interface motion is slow enough (Aziz, 1988). When this  
427 is the case, the chemical potentials of ions at the surface  
428 of the particle are equal to those in the aqueous solu-  
429 tion. The composition  $x$  of the layer which is deposited  
430 is obtained from the condition that  $\delta \Delta G(x)$  is minimum  
431 with respect to  $x$ . The  $x$  dependence of  $\delta \Delta G(x)$  is in-  
432 cluded in  $-\ln I(x)/v(x)$ . Determining the composition

433  $x$  of the incremental layer thus amounts to minimizing  
434 this quantity. Because it is the same quantity which ap-  
435 pears in the determination of the critical nucleus compo-  
436 sition, the composition of the incremental layer at time  $t$   
437 is thus equal to  $x^*(t)$ .

Usually, and especially at low temperatures, solid state  
diffusion is very slow compared to all other characteristic  
times. We will neglect it, and assume that the composi-  
tion of a given layer remains fixed once formed (Doerner-  
Hoskins precipitation (Doerner and Hoskins, 1925)). The  
particles thus display composition profiles due to the time  
variation of  $x^*$ .

The dimensions and number of growth units of a par-  
ticle at time  $t$  depend on two time indices:  $t_1$  the time at  
which the particle has nucleated, and  $t$  the time of ob-  
servation. One has thus to write:  $n(t_1, t)$  and  $\rho(t_1, t)$  ( $\rho$   
the radius of the particle). At variance, the composition  
of the outer layer of growing particles only depends on  $t$ ,  
because it is the same for all particles.

In the regime of increasing particle size  $d\rho(t_1, t)/dt >$   
0, the growth equation used for particles of fixed composi-  
tion can be straightforwardly generalized to SSs (Noguera  
et al. 2010):

$$\frac{d\rho(t_1, t)}{dt} = \kappa \left( I(t, x^*(t)) - \exp \left[ \frac{2u(x^*(t))}{n(t_1, t)} \right]^{1/3} \right) \quad (20)$$

In Eq. 20, it is the saturation index relative to the com-  
position of the deposited layer, and thus relative to a SS  
of composition  $x^*(t)$ , which must be used.

##### B. Redissolution

417 Whenever the right hand-side of Eq. 20 is negative, i.e.  
418 whenever  $n(t_1, t) < n^*(t)$ , the particles decrease in size  
419 ( $d\rho(t_1, t)/dt < 0$ ). During such a redissolution stage, lay-  
420 ers formed at anterior times are progressively dissolved.  
421 A layer corresponding to a radius  $\rho(t_1, t)$  which reaches  
422 the particle/solution interface at time  $t$ , had been de-  
423 posited at time  $t_2$  such that:

$$\rho(t_1, t_2) = \rho(t_1, t) \quad (21)$$

$t_2$  is specific to the particle and thus depends on  $t_1$  and  
 $t$ . At time  $t_2$ , the layer composition was equal to  $x^*(t_2)$ .  
Consequently, in the redissolution regime, the growth  
rate reads:

$$\frac{d\rho(t_1, t)}{dt} = \kappa \left( I(t, x^*(t_2)) - \exp \left[ \frac{2u(x^*(t_2))}{n(t_1, t)} \right]^{1/3} \right) \quad (22)$$

As a whole, the growth laws written in Eqs. 20 and 22  
allow positive or negative growth of particles, depending  
on the relative value of their size with respect to the  
critical nucleus size. The process of Ostwald ripening is  
thus included in the present formalism. At variance, a

476 growth law of the type:

$$\frac{d\rho(t_1, t)}{dt} = \kappa(I^p(t, x(t_1, t)) - 1)^q \quad (23)$$

477 as often assumed in the literature (Lasaga, 1984; 524  
478 Parkhurst and Appelo, 1999), is unable to lead the solid 525  
479 phase toward equilibrium, whatever the values of the em- 526  
480 pirical exponents  $p$  and  $q$ . In the long term, it correctly 527  
481 drives the saturation state of the AS towards 1 if the 528  
482 feed-back effect of growth on the AS composition is in- 529  
483 cluded, but because all nucleated particles survive, the 530  
484 total surface energy of the solid phase is not minimized. 531  
485 The lowest energy configuration (a single particle with 532  
486 all available matter in it) is never reached. 533

## 487 V. FEED-BACK EFFECT ON THE SOLUTION 534

488 At a given time  $t$ , the particle population consists of all 536  
489 the particles which have nucleated at times  $t_1 < t$ , and 537  
490 with nucleation frequencies and sizes equal to  $F(t_1)$  and 538  
491  $n(t_1, t)$  respectively. The amounts  $q_M(t)$  of end-members 539  
492 M (M=AC or BC) which have been withdrawn from the  
493 AS at time  $t$  are thus equal to:

$$q_M(t) = \int_0^t F(t_1)(n^*(t_1) - 1)X_M(t_1)dt_1 + \int_0^t F(t_1)dt_1 \int_{t_1}^t dt_3 \frac{dn(t_1, t_3)}{dt_3} X_M(t_3) \quad (24)$$

494 The first term represents the contribution of nucle- 546  
495 ation, with  $X_M(t_1)$  the molar fractions of the end- 547  
496 members equal to  $(1 - x^*(t_1))$  and  $x^*(t_1)$  for M=AC and 548  
497 BC, respectively. The second term is due to the size evo- 549  
498 lution of the particles.  $n^*(t_1) - 1$  is written rather than 550  
499  $n^*(t_1)$  to signal that more than one growth unit is neces- 551  
500 sary to determine if a solid phase is formed. In the case of 552  
501 redissolution  $X_M(t_3)$  must be put equal to  $X_M(t_2)$  with 553  
502  $t_2$  determined by the condition that  $\rho(t_1, t_2) = \rho(t_1, t_3)$  554  
503 (Equation 21). From these quantities and an ionic spe- 555  
504 ciation model, one can calculate all activities in the AS 556  
505 and the saturation indexes  $I_{AC}(t)$ ,  $I_{BC}(t)$  and  $I(t, x)$ . 557

506 Including feed-back effects on the AS allows an evolu- 558  
507 tion of its composition towards thermodynamic equilib- 559  
508 rium. When  $t \rightarrow \infty$ ,  $I(t, x^*)$  tends to 1 and, combining 560  
509 Equations 5 and 16, it is easy to check that  $x^* \rightarrow x_0$ , as 561  
510 it should. 562

511 The equation giving  $q_M(t)$  (Equation 24), together 563  
512 with those which fix  $I(t, x)$ ,  $x^*(t_1)$ ,  $n^*(t_1)$ ,  $\Delta G^*(t_1)$ , 564  
513  $F(t_1)$ , and  $\rho(t_1, t)$  form a complete set which, together 565  
514 with the speciation equations, allow the full determina- 566  
515 tion of the precipitate and aqueous solution characteris- 567  
516 tics at all times. 568

517 The present formalism represents an important ad- 569  
518 vance with respect to our previous work (Noguera et 570  
519 al., 2010) which was restricted to ideal solid solutions, 571

spherical particles and homogeneous nucleation. The de-  
velopment of the NANOKIN code to include these new  
functionalities is presently under progress, and its ap-  
plication to a realistic precipitation process will be the  
subject of a forthcoming paper. In the following, we will  
highlight some generic characteristics of the precipitation  
of non-ideal SS, and, under some approximations, we will  
present some numerical simulations exemplifying various  
scenarios which may be encountered in the precipitation  
of SSs of geochemical interest.

## VI. PRECIPITATION SCENARIOS

In this section, we first discuss the characteristics of  
the precipitation process as a function of the degree of  
non-ideality of the SS and we evidence four possible pre-  
cipitation scenarios (Section VIA). We then discuss their  
conditions of occurrence, under some simplifying assump-  
tions, and we represent them graphically as a function of  
the ratio of the solubility products of the end-members  
and the Guggenheim coefficient  $A_0$  (Section VIB).

### A. The four scenarios

540 First we recall that when the Guggenheim coefficients  
541  $A_0$  and  $A_1$  belong to the zone included in between the two  
542 lines drawn in Figure 3 (lower panel), the equations which  
543 fix  $x_{st}$  and  $x^*$  have a single root and the precipitation  
544 scenario bears strong resemblances to that of an ideal  
545 SS. When  $A_0 > 0$ , the only difference with truly ideal  
546 SSs lies in the corrections due to the activity coefficients  
547  $\lambda_{AC}$  and  $\lambda_{BC}$ . In that case the precipitation scenario  
548 will be called *Precipitation Scenario #1* (Sc. #1).

549 When the contribution of the enthalpy of mixing of the  
550 SS to the Gibbs free energy of dissolution is negative, the  
551 SS displays a tendency towards ordering. It is generally  
552 associated with negative values of the first Guggenheim  
553 coefficient <sup>1</sup> and is usually interpreted as resulting from  
554 short range attraction between dissimilar first neighbors,  
555 which favors A-B pairs over A-A or B-B pairs. Which  
556 order is actually achieved depends on a contribution of  
557 the entropy of mixing which is specific to each case. Be-  
558 cause at the present stage our study remains generic, we  
559 do not introduce it, so that this limit is not well-treated  
560 by our approach and will not be further discussed.

561 In the limit of strong non-ideality of the SS, a miscibil-  
562 ity gap is present which is revealed by a jump of  $x^*$  from  
563  $x_1$  to  $x_2$  at a critical value  $W'_c$  of  $W' = I_{BC}/I_{AC}^z$  (see e.g.  
564 Figure 5). This occurs when the Guggenheim coefficients  
565  $A_0$  and  $A_1$  belong to the regions of the diagram in Figure  
566 3 above or below the two lines.  $x_1$ ,  $x_2$  and  $W'_c$  are solely  
567 determined by the values of  $A_0$ ,  $A_1$  and  $z = v_{BC}/v_{AC}$   
568 (See Appendix D). For example, in the special case where  
569  $A_1 = 0$  (regular SSs) and  $z = 1$ ,  $x_2$  is equal to  $1 - x_1$   
570 and the critical value for  $W$  is equal to  $W'_c = 1$  (see Sec-  
571 tions 2 and 3). The question of phase separation in the

<sup>1</sup> For sub-regular SSs, the  $A_1$  coefficient should also be taken into account. However, in the logics of the Guggenheim expansion and its truncation,  $A_1$  is expected to be smaller than  $A_0$ , in absolute value, so that extension of the zone of existence of a miscibility gap towards negative  $A_0$  values in Figure 3 appears meaningless.

critical nuclei or in the deposited layers becomes relevant only when  $W' = W'_c$  because then the nucleation barrier (Eq. 14) takes equal values for  $x^* = x_1$  and  $x^* = x_2$  and the same is true for the interfacial Gibbs free energy for growth (Eq. 19).

Consequently, the scenario of precipitation depends on whether and how the condition  $W' = W'_c$  is met during the time evolution of the system. The initial conditions (embedded in the value of  $W'$  at time  $t = 0$ ) and the sign of  $dW'/dt$  in the vicinity of the discontinuity are the relevant factors in that respect. We first note that, in the presence of a miscibility gap,  $W'(t)$  has a slope discontinuity at  $W' = W'_c$ , due to the different values  $x_1$  and  $x_2$  of the SS composition for  $W' < W'_c$  and  $W' > W'_c$ , respectively (Appendix E). We will note  $dW'_1/dt$  and  $dW'_2/dt$  the associated two time derivative values of  $W'(t)$ , respectively. This allows discrimination of the following scenarios:

- conditions are such that during the precipitation process the discontinuity is not met. This takes place if, at  $t = 0$ ,  $W' < W'_c$  and close to the discontinuity  $dW'_1/dt < 0$ , or if, at  $t = 0$ ,  $W' > W'_c$  and close to the discontinuity  $dW'_2/dt > 0$ . This scenario will be referred to, in the following, as *Precipitation Scenario #2* (Sc. #2).
- conditions are such that, during the precipitation process, the discontinuity is met but  $dW'/dt$  has the same sign on both sides of the discontinuity. The discontinuity is thus crossed but the time spent by the system at  $W' = W'_c$  is irrelevant. No phase separation takes place. This scenario will be referred to as *Precipitation Scenario #3* (Sc. #3).
- finally, it may be that the discontinuity is met but  $dW'/dt$  has opposite signs on both sides of the discontinuity, which tends to bring it back towards  $W' = W'_c$  on both sides. There is then a conflict between the variations of  $W'$  forcing it to stay constant and equal to  $W'_c$  (Lyapunov stable equilibrium point (Lyapunov, 1992)). It is in this case that phase separation takes place, in order to allow the condition  $dW'/dt = 0$  to be fulfilled. This scenario will be referred to as *Precipitation Scenario #4* (Sc. #4).

To go further, one has to determine the sign of  $dW'/dt$  on the left and right of the discontinuity. It is possible to derive formal expressions for  $dW'_1/dt$  and  $dW'_2/dt$  from the feed-back equations, as described in Appendix E, and also to deduce the relative percentages  $\alpha$  and  $(1 - \alpha)$  of the two SSs with composition  $x_1$  and  $x_2$  when phase separation occurs. These expressions may then be quantitatively estimated for specific cases.

Aside from this numerical approach, in the following in order to gain some physical insight into practical conditions of occurrence of the four scenarios, we restrict the discussion to regular SSs and some simplified conditions of precipitation. This will allow us to devise a dia-

gram of occurrence of the scenarios as a function of some parameters (ratios of the solubility products of the two end-members, degree  $A_0$  of non-ideality of the SS and initial conditions of precipitation), and to make qualitative predictions of the precipitation characteristics of realistic SSs of geochemical interest.

## B. Conditions of existence of the four scenarios for regular SSs

The simplifying assumptions are the following:

- the SS is regular ( $A_1 = 0$ )
- the formula unit volume as well as the surface energy of the SS are assumed to be independent of  $x$ . For example they may be set equal to the average of the corresponding values of the end-members. Consequently, there are no surface excess quantities (Appendix C) and  $z = 1$ .
- the A, B and C species are the dominant forms of the elements in the AS, and no mineral other than the SS may dissolve or precipitate. The time evolution of the [A], [B] and [C] activities thus only comes from the precipitation of the SS under consideration. Moreover, for SSs with a miscibility gap, we assume that, at the time when the  $x^*$  discontinuity is met, redissolution is negligible. Both hypotheses imply that the contribution  $W''$  to  $dW'/dt$  which is continuous at  $W'_c$  vanishes (Appendix E).

Under these hypotheses, in strongly non-ideal SSs ( $A_0 > 2$ ), the miscibility gap is symmetric ( $x_2 = 1 - x_1$ ) and  $W'_c = 1$ . At the discontinuity, the last equality means that  $[B]/[A] = K_{BC}/K_{AC}$ . Moreover, close to the discontinuity (Appendix E):

$$\frac{1}{W'} \frac{dW'}{dt} \propto - \left( x^*(t) - (1 - x^*(t)) \frac{K_{BC}}{K_{AC}} \right) \quad (25)$$

with  $x^*$  equal to  $x_1$  or  $x_2$  when  $W'_c$  is smaller or larger than 1, respectively.

As a consequence:

- $dW'_1/dt > 0$  if  $x_1/(1 - x_1) < K_{BC}/K_{AC}$
- $dW'_1/dt < 0$  otherwise
- $dW'_2/dt > 0$  if  $x_2/(1 - x_2) < K_{BC}/K_{AC}$
- $dW'_2/dt < 0$  otherwise

Using these inequalities, the conditions of occurrence of Scenario #2 read:

$$\frac{[B(t=0)]}{[A(t=0)]} < \frac{K_{BC}}{K_{AC}} < \frac{x_1}{1 - x_1} \quad (26)$$

669 OR:

$$\frac{x_2}{1-x_2} < \frac{K_{BC}}{K_{AC}} < \frac{[B(t=0)]}{[A(t=0)]} \quad (27)$$

670 Scenario #3 requires that the three ratios  $[B(t=0)]/[A(t=0)]$ ,  $x_1/(1-x_1)$  and  $x_2/(1-x_2)$  are simultaneously either smaller than  $K_{BC}/K_{AC}$  or larger than it. Finally, Scenario #4 takes place when the following inequalities are fulfilled:

$$\frac{x_1}{1-x_1} < \frac{K_{BC}}{K_{AC}} < \frac{x_2}{1-x_2} \quad (28)$$

675 whatever the value of  $[B(t=0)]/[A(t=0)]$

676 These conditions are graphically represented in Figure 6, as a function of  $\ln K_{BC}/K_{AC}$  and the degree  $A_0$  of non-ideality of the SS. The boundaries between the zones of existence of the scenarios #1, #2, #3, and #4 include the vertical line  $A_0 = 2$  on the left of which only Scenario #1 takes place, and the two lines  $\ln K_{BC}/K_{AC} = \ln x_1/(1-x_1)$  and  $\ln K_{BC}/K_{AC} = \ln x_2/(1-x_2)$ . In between the two latter, phase separation takes place within Scenario #4.

677 Outside these regions, Scenarios #2 or #3 may take place, depending on the initial conditions. When  $\ln K_{BC}/K_{AC} > \ln x_2/(1-x_2)$ , the discontinuity is not crossed (Scenario #2) if  $[B(t=0)]/[A(t=0)] > K_{BC}/K_{AC}$  and otherwise it is crossed (Scenario #3). Symmetrically, when  $\ln K_{BC}/K_{AC} < \ln x_2/(1-x_2)$ , the discontinuity is not crossed (Scenario #2) if  $[B(t=0)]/[A(t=0)] < K_{BC}/K_{AC}$  and otherwise it is crossed (Scenario #3). The difference between the two scenarios, i.e. the existence of a composition discontinuity inside the particles, is thus only fixed by the initial conditions in these regions.

## 697 VII. NUMERICAL SIMULATION AND RELEVANT EXAMPLES

698 In this section, we present results of numerical simulations which highlight the generic characteristics of the precipitation kinetics under conditions such that scenarios #1, #2, #3 or #4 take place. We will make use of the same assumptions as in subsection VIB and also assume that the particles have a spherical shape. Although these assumptions are rather simplistic, they help provide a first insight into the precipitation characteristics of SSs of geochemical interest.

### 708 A. Weakly non-ideal SS: precipitation Scenario #1

709 When the Guggenheim coefficient  $A_0 < 2$ , the SS which forms is weakly non-ideal. The only difference from truly ideal SSs lies in the corrections due to the activity coefficients  $\lambda_{AC}$  and  $\lambda_{BC}$ . The dynamics of precipitation presents many common characteristics with that of ideal

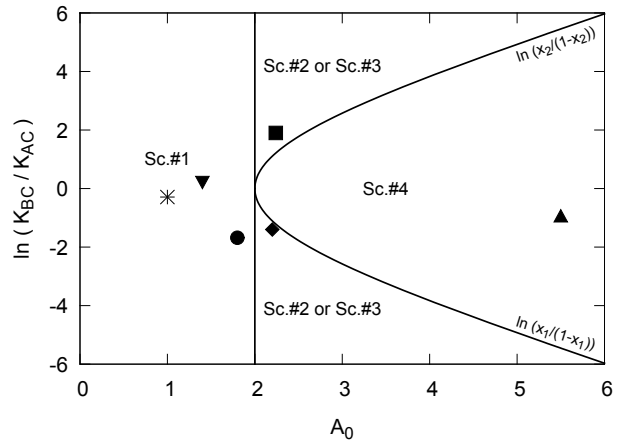


FIG. 6: Diagram  $\ln K_{BC}/K_{AC}$  as a function of the degree  $A_0$  of non-ideality of the SS, representing the zones of existence of the scenarios #1, #2, #3, and #4.  $K(\text{Cl,Br})$ ,  $(\text{Mg,Fe})\text{CO}_3$ ,  $(\text{Ba,Ra})\text{SO}_4$ ,  $(\text{Ca,Zn})\text{CO}_3$ ,  $\text{Ca}(\text{SO}_4, \text{SeO}_4)$  and  $(\text{Ca,Sr})\text{CO}_3$  SSs are located in this diagram, represented by triangle-down, circle, star, diamond, square and triangle-up, respectively (see text).

SSs, which we have analyzed in a previous work (Noguera et al., 2010). Two typical examples are shown in Figure 7, for  $A_0 = 1$  and two values of the solubility product ratio  $K_{BC}/K_{AC}$ .

In both cases, due to nucleation and growth, the AS is impoverished in A, B, and C species as time passes and  $I(t, x^*(t))$  decreases towards 1, until thermodynamic equilibrium is reached in the long term. The time variation of the critical nucleus composition is very dependent on the ratio  $K_{BC}/K_{AC}$ . When the solubility products of the two end-members are close to each other, the range of  $x^*$  values is small and the composition profile of the particles is smooth, as exemplified in Figure 7 (left panels) where  $K_{BC}/K_{AC}$  was chosen equal to 1. At variance, when the two end-members have largely different solubility products,  $x^*$  varies in a larger range as shown in Figure 7 (right panels) for which  $K_{BC}/K_{AC} = 10$ . The surviving particles may display either a core-shell structure, with a smooth interface between core and shell, or nearly constant composition, depending on the initial conditions. In any case, when thermodynamic equilibrium is reached, the last surviving particle has a non-homogeneous composition, at variance with thermodynamic models of SSs which assume an homogeneous composition.

$\text{KCl}_{1-x}\text{Br}_x$  was shown to be a quasi-regular SS, with  $A_0 = 1.4$  and a very small  $A_1$  coefficient (Glynn et al., 1990) and the two end-members have a small solubility product ratio ( $K_{BC}/K_{AC} = 1.68$  (Blanc et al., 2012)). The particles formed during precipitation are thus expected to have a smooth composition profile. This is also the case for the  $(\text{Ba,Ra})\text{SO}_4$  SS with a ratio of solubility products  $K_{BC}/K_{AC}$  equal to 0.512 (Hummel

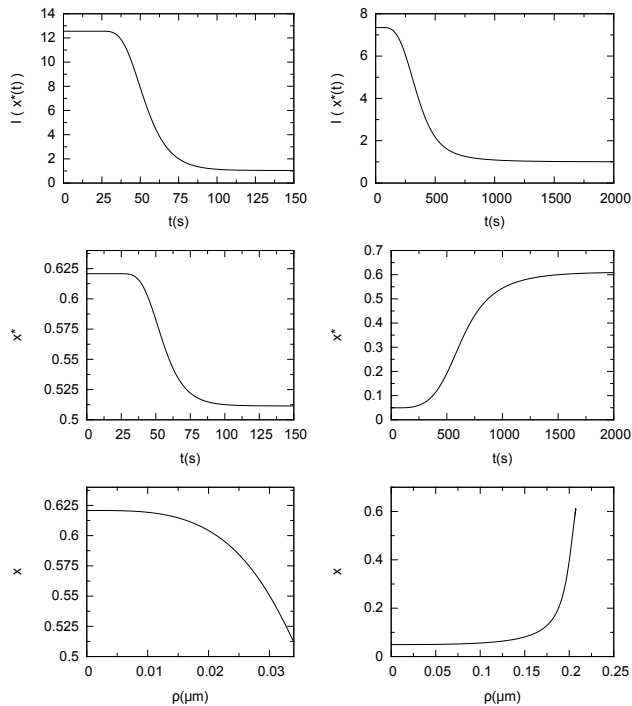


FIG. 7: From top to bottom: time dependence of the saturation state  $I(t, x^*(t))$ , time dependence of the critical nucleus composition  $x^*$  and concentration profile of the surviving particles at the end of the simulation. Left and right panels refer to  $K_{BC}/K_{AC} = 1$  and 10, respectively. All curves have been drawn for  $A_0 = 1$ ,  $A_1 = 0$ ,  $F_0 = 10^{19}$  particles per second and liter of solution,  $\sigma = 50$  mJ/m<sup>2</sup> independent on composition,  $\kappa = 10^{-10}$  m/s,  $v_{AC} = v_{BC} = 50$  Å<sup>3</sup>,  $K_{AC} = 10^{-6}$  and initial activities:  $[A(t=0)] = 7.10^{-4}$ ,  $[B(t=0)] = 9.10^{-4}$ ,  $[C(t=0)] = 10^{-2}$ .

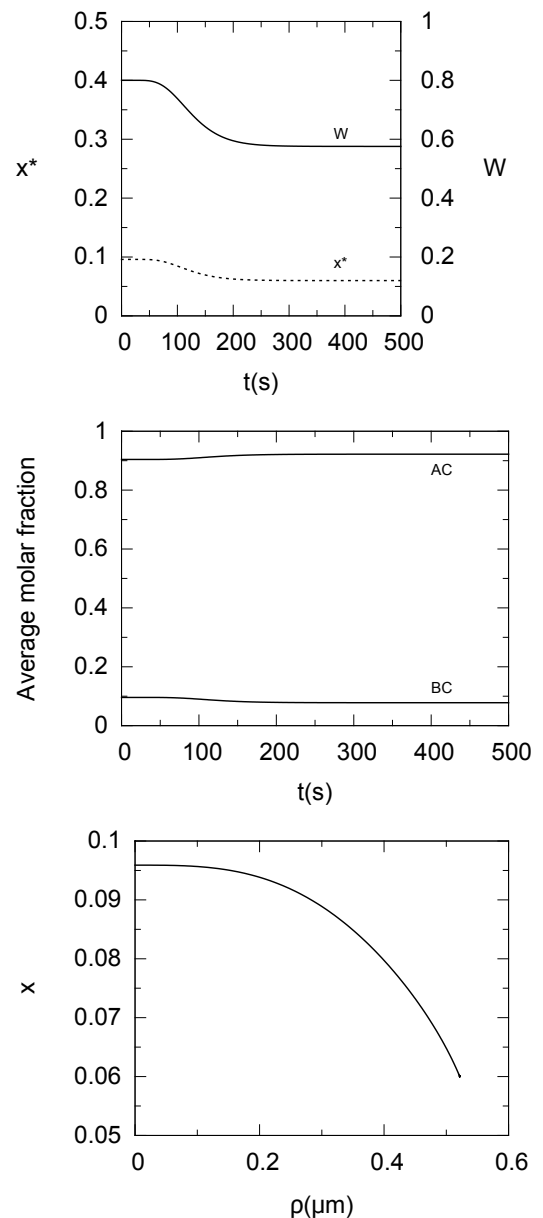


FIG. 8: From top to bottom: time dependence of  $W$  and the critical nucleus composition  $x^*$ , time dependence of the end-member average molar fractions  $q_{AC}/(q_{AC} + q_{BC})$  and  $q_{BC}/(q_{AC} + q_{BC})$ , and composition profile of long lasting particles. All curves have been drawn for  $A_0 = 2.5$ ,  $A_1 = 0$ ,  $F_0 = 10^{19}$  particles per second and liter of solution,  $\sigma = 50$  mJ/m<sup>2</sup> independent on composition,  $\kappa = 10^{-9}$  m/s,  $v_{AC} = v_{BC} = 50$  Å<sup>3</sup>,  $K_{AC} = 10^{-6}$ ,  $K_{BC} = 10^{-7}$  and initial activities:  $[A(t=0)] = 6.10^{-4}$ ,  $[B(t=0)] = 48.10^{-6}$ ,  $[C(t=0)] = 10^{-2}$ .

747 et al., 2002). This SS has recently been studied by  
 748 Brandt et al. (2015) who confirmed a Guggenheim co-  
 749 efficient  $A_0 = 1$  as theoretically predicted (Vinograd et  
 750 al., 2013). At variance, particles of  $\text{Mg}_{1-x}\text{Fe}_x\text{CO}_3$ , for  
 751 which  $A_0 = 1.8$  (Chai and Navrotsky, 1996) should dis-  
 752 play a core-shell structure because the solubility products  
 753 of the end-members differ by about two orders of magni-  
 754 tude ( $K_{BC}/K_{AC} = 0.02$  (Blanc et al., 2012)). The infor-  
 755 mation for the three SSs described above are reported in  
 756 Figure 6.

## 757 B. Strongly non-ideal SS: precipitation Scenario 758 #2 without composition discontinuity

759 We present here simulation results for the precipita-  
 760 tion of a strongly non-ideal SS ( $A_0 = 2.5$ ,  $x_1 = 0.1448$   
 761 and  $x_2 = 0.8552$ ), under conditions relevant for scenario  
 762 #2 (Conditions 26 or 27). In Figure 8, initial conditions  
 763 and ratios of solubility products have been chosen such  
 764 that  $W' < 1$  at  $t = 0$  and  $dW'_1/dt < 0$ . The system  
 765 thus does not encounter the composition discontinuity  
 766 and the time dependence of  $x^*$  is smooth. The critical

nuclei and the deposited layers remain AC rich during the whole precipitation process, consistent with average molar fractions of the AC and BC end-members in the precipitate,  $q_{AC}/(q_{AC} + q_{BC})$  and  $q_{BC}/(q_{AC} + q_{BC})$ , close to 90% and 10%, respectively. A typical particle composition profile at the end of the process is shown in Figure

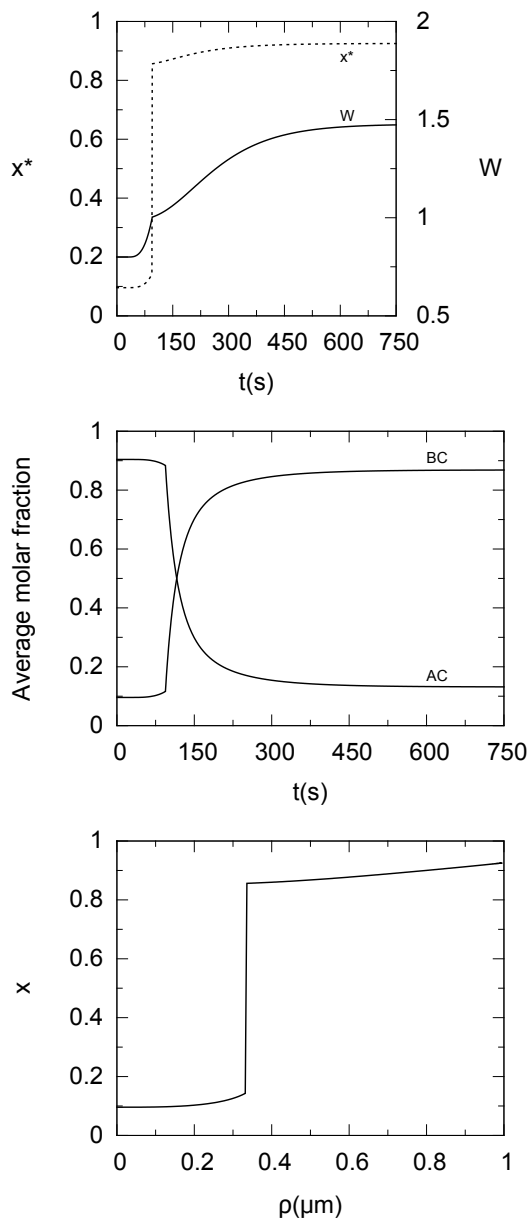


FIG. 9: From top to bottom: time dependence of  $W$  and the critical nucleus composition  $x^*$ , time dependence of the end-member average molar fractions  $q_{AC}/(q_{AC} + q_{BC})$  and  $q_{BC}/(q_{AC} + q_{BC})$ , and composition profile of long lasting particles. Same parameter values as in Figure 8, except  $K_{BC} = 10^{-5}$  and  $[B(t=0)] = 48.10^{-4}$ .

### C. Strongly non-ideal SS: precipitation Scenario #3 with a crossing of the composition discontinuity

This is another example of precipitation of a strongly non-ideal SS, with the same characteristics as the previous one ( $A_0 = 2.5$ ,  $x_1 = 0.1448$  and  $x_2 = 0.8552$ ), but under conditions relevant for scenario #3, i.e. such that the discontinuity in the  $x^*$  versus  $W'$  curve is met and crossed (same sign of  $dW'/dt$  on both sides of the discontinuity).

The precipitation characteristics shown in Figure 9 have been obtained under conditions close to those of the previous subsection, except for the initial activity  $[B(t=0)]$  and for the ratio of solubility products. At  $t = 0$ ,  $W' < 1$  and  $dW'_1/dt > 0$ . The system thus meets the composition discontinuity at the time  $t_c$  when  $W' = 1$ . This clearly shows up in the time dependence of  $x^*$  which displays a 70% jump, and in the slope discontinuity in the time dependence of  $W'$ . Before  $t_c$ , the critical nucleus and deposited layer compositions are AC rich ( $x \approx 15\%$ ). They become BC rich ( $x \approx 85\%$ ) after  $t_c$ . This sudden change is reflected in the time dependence of the molar fractions of the end-members in the precipitate which displays a crossing point at some time posterior to  $t_c$ . The composition profile of the particles at the end of the process also reflects the discontinuity which has occurred at  $t_c$ . The particles have a core-shell structure, with an AC-rich core and a BC-rich shell and an abrupt interface between core and shell (Figure 9, bottom panel).

$\text{Ca}_{1-x}\text{Zn}_x\text{CO}_3$  and  $\text{Ca}(\text{SO}_4)_{1-x}(\text{SeO}_4)_x$  SSs may display precipitation scenarios #2 or #3 depending on the initial value of the  $[\text{Zn}]/[\text{Ca}]$  or  $[\text{SeO}_4]/[\text{SO}_4]$  activity ratios. Indeed, for both SSs, the Guggenheim coefficients  $A_0$  are equal to 2.2 (Glynn and Reardon, 1990) and 2.24 (Fernández-González et al., 2006), respectively, and their solubility products locate them, respectively, in the lower and upper regions of Figure 6 where scenarios #2 or #3 take place. ( $K_{BC}/K_{AC} = 0.03$  for  $\text{Ca}_{1-x}\text{Zn}_x\text{CO}_3$  (Crocket and Winchester, 1966) and  $K_{BC}/K_{AC} \approx 80$  for  $\text{Ca}(\text{SO}_4)_{1-x}(\text{SeO}_4)_x$  (Parkhurst and Appelo, 1999)). During their formation by precipitation, the particles are thus expected to display smooth profiles or core-shell structure depending on initial conditions which will determine whether scenarios #2 or #3 apply.

### D. Strongly non-ideal SS: precipitation Scenario #4 with phase separation

Keeping the characteristics of the SS unchanged with respect to the two previous subsections ( $A_0 = 2.5$ ,  $x_1 = 0.1448$  and  $x_2 = 0.8552$ ), we now consider conditions relevant for scenario #4, i.e. such that the discontinuity is met but  $dW'/dt$  has opposite signs on both sides of the discontinuity. This happens if, at  $t = 0$ ,  $W' < 1$  and close to the discontinuity  $dW'_1/dt > 0$  and  $dW'_2/dt < 0$ , or if, at  $t = 0$ ,  $W' > 1$  and close to the discontinuity

8 bottom panel. The particles are non-uniform in com-  
position and become more AC-rich close to their surface.  
However, the variation of composition  $x$  between the core  
and the surface is small, of the order of 4%.

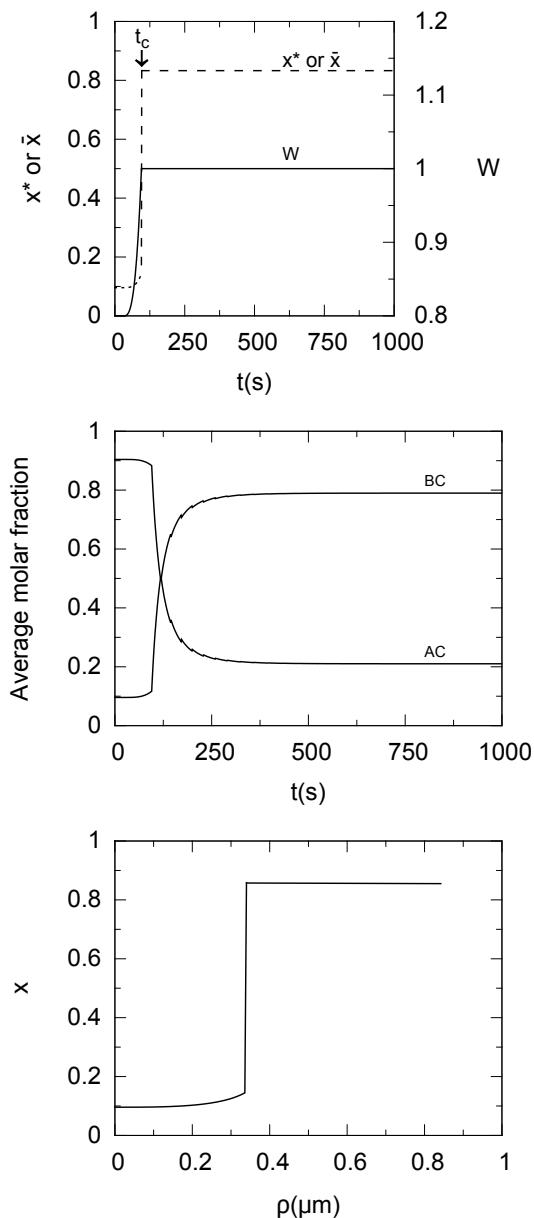


FIG. 10: From top to bottom: time dependence of  $W$ , time dependence of the critical nucleus composition  $x^*$  (when  $t < t_c$ ) or  $\bar{x} = \alpha x_1 + (1 - \alpha)x_2$  (when  $t > t_c$ ); time dependence of the end-member average molar fractions  $q_{AC}/(q_{AC} + q_{BC})$  and  $q_{BC}/(q_{AC} + q_{BC})$ ; composition profile of a long lasting particle. Same parameter values as in Figure 8, except  $K_{BC} = 5.10^{-6}$  and  $[B(t=0)] = 24.10^{-4}$ .

$dW'_1/dt < 0$  and  $dW'_2/dt > 0$  (Condition 28).

For the example shown in Figure 10, initial conditions and ratios of solubility products have been chosen so that  $W' < 1$  at  $t = 0$ , and simultaneously  $dW'_1/dt > 0$  and  $dW'_2/dt < 0$  at the discontinuity. All other parameters are equal to those of the preceding examples. The system encounters the composition discontinuity at a time  $t_c$ . The conflicting variations of  $W'$  on the left and right of the discontinuity force  $W'$  to remain constant and equal

to 1 at all posterior times (Figure 10, top panel). For all times  $t > t_c$ , the ratio of B and A activities remains constant ( $[B(t)]/[A(t)] = K_{BC}/K_{AC}$ ), although the saturation states  $I_{AC}$  and  $I_{BC}$  of the AS with respect to the end-members decrease. Phase separation between phases of compositions  $x_1$  and  $x_2$  takes place at  $t > t_c$ , with relative amounts  $\alpha$  and  $1 - \alpha$  (Eq. 61 in Appendix E). It is not easy to tell how the two phases will be spatially organized, but an average composition in the critical nucleus or the instantaneous deposited layers may be defined at each time  $t > t_c$  as  $\bar{x} = \alpha x_1 + (1 - \alpha)x_2$ . Because  $\alpha$  remains constant, the same is true for  $\bar{x}$ , which in the present example is equal to 0.833. Because it is closer to  $x_2$  than to  $x_1$ , the end-member molar fractions  $q_{AC}/(q_{AC} + q_{BC})$  and  $q_{BC}/(q_{AC} + q_{BC})$  strongly vary for  $t > t_c$  and tend to approximately  $1 - \alpha$  and  $\alpha$ , respectively, in the long term. A typical particle profile is shown in the lowest panel of Figure 10, highlighting a core-shell structure and an abrupt interface between them.

$\text{Ca}_{1-x}\text{Sr}_x\text{CO}_3$  is a strongly non-ideal SS characterized by a Guggenheim coefficient equal to 5.5 (Casey et al., 1996), indicating poor solubility of Sr in aragonite and a miscibility gap occupying most of the phase diagram ( $x_1 \approx 0.004$  and  $x_2 \approx 0.996$ ). Whatever the initial conditions of precipitation, a phase separation is expected, as in the example shown in Figure 10.

## VIII. CONCLUSION

We have developed a formalism which describes the precipitation kinetics of non-ideal SSs from an initially supersaturated AS. It treats the time evolution of the AS composition and the formation, growth or redissolution of particles. It extends our previous work, which was restricted to ideal SSs, spherical particles and homogeneous nucleation. The formalism is relevant to both mineral SSs and bimetallic nanoparticle formation. To our knowledge, it is the first time, in the fields of both geochemistry and metallic alloys, that these out-of-equilibrium processes are fully taken into account for non-ideal SSs.

This work highlights how particle composition and size vary with time, resulting in composition profiles which may be smooth or discontinuous, depending on the Guggenheim parameter values which drive the non-ideality of the SSs, and the ratio of the solubility products of the end-members. We have shown that even for strongly non-ideal SSs, phase separation is not the general case and that other scenarios may take place. We have specified their characteristics and under which conditions they may be encountered. Numerical simulations have been performed to exemplify them for a regular SS, under a few simplifying assumptions, and qualitative predictions of the precipitation characteristics of some mineral SSs have been made.

The development of the NANOKIN code to include these new functionalities is presently under progress, and its application to a realistic precipitation process will be

895 the subject of a forthcoming paper. In the context of  
 896 water-rock interactions, our work provides enhanced possibilities  
 897 for analyzing precipitation processes for various  
 898 SS types, such as carbonates, sulfates or clay minerals,  
 899 among others.

### 900 Appendix A: Condition of stoichiometric saturation

901 In this appendix, we analyze the mathematical properties  
 902 of the function  $-\ln I(x) = \ln K(x) - \ln Q(x)$  whose  
 903 minimum determines the stoichiometric saturation condition  
 904 (Eq. 10 in the text).  $-\ln I(x)$  reads:  
 905

$$\begin{aligned} -\ln I(x) = & -(1-x)\ln I_{AC} - x\ln I_{BC} \\ & +x(1-x)[A_0 + A_1(2x-1)] \\ & +x\ln x + (1-x)\ln(1-x) \end{aligned} \quad (29)$$

906 or:

$$\begin{aligned} -\ln \frac{I(x)}{I_{AC}} = & -x\ln W + x(1-x)[A_0 + A_1(2x-1)] \\ & +x\ln x + (1-x)\ln(1-x) \end{aligned} \quad (30)$$

907 after introducing the ratio  $W$  of the saturation states of  
 908 the AS with respect to the pure end-members:

$$W = \frac{I_{BC}}{I_{AC}} \quad (31)$$

909 In the following we analyze the variations of the function  
 910  $f(x)$  equal to the right hand side of Eq. 30. Its first  
 911 derivative is:

$$\frac{df(x)}{dx} = \ln \frac{x}{W(1-x)} + A_0(1-2x) - A_1(1-6x+6x^2) \quad (32)$$

912 and its second derivative is:

$$\frac{d^2f(x)}{dx^2} = -2A_0 + 6A_1(1-2x) + \frac{1}{x} + \frac{1}{1-x} \quad (33)$$

913 There are regions of the parameter space  $\{A_0, A_1\}$   
 914 where  $d^2f(x)/dx^2 > 0$  whatever  $x$ . In that case,  $f(x)$   
 915 is a convex function, with a single minimum. This happens,  
 916 for example when  $A_1 = 0$  and  $A_0 < 2$ . Otherwise,  
 917  $f(x)$  may display one minimum, or two minima and a  
 918 maximum, depending upon the value of  $W$ .

919 Figure 11 exemplifies this latter case when  $A_0 = 2.5$   
 920 and  $A_1 = 0$ . At low or high values of  $W$  (typically less  
 921 than 0.86 or more than 1.14),  $f(x)$  has a single minimum  
 922 at  $x$  smaller or larger than 0.5, respectively. For inter-  
 923 mediate values of  $W$ ,  $f(x)$  has two minima. The composition  
 924  $x_{st}$  which corresponds to stoichiometric saturation  
 925 is the one for which  $f(x)$  is the lowest.  $x_{st}$  displays a discontinuity  
 926 between  $x_1$  and  $x_2$  at a critical value  $W_c = 1$   
 927 for which  $f(x_1) = f(x_2)$ . This behavior is represented in  
 928 Figure 1 in the main text.

929 Similar reasoning for different values of  $A_0$  and  $A_1$   
 930 leads to Figure 2, which shows that  $W_c$  remains equal

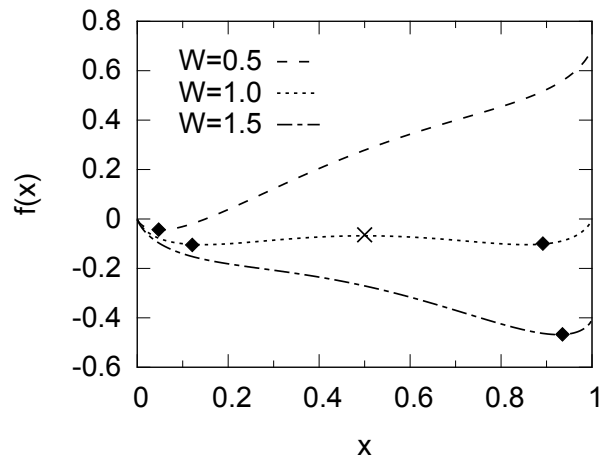


FIG. 11: Curve representative of  $f(x)$  (right hand side of Eq. 30) for  $A_0 = 2.5$ ,  $A_1 = 0$  and  $W = 0.5, 1.$  and  $1.5$ . The three curves exemplify the cases when  $f(x)$  presents a single minimum at small value of  $x$ , two degenerate minima or a single minimum at large  $x$  value. The diamonds on the curves mark the positions of the minima and the cross the maximum.

931 to 1 whatever the value of  $A_0 > 2$  if  $A_1 = 0$ , but varies  
 932 with  $A_0$  when  $A_1 \neq 0$ .

933 Finally, the limiting values of  $A_0$  and  $A_1$  between regions  
 934 of discontinuities in  $x_{st}$  and regions where it varies smoothly,  
 935 are obtained from the condition that simultaneously  $d^2f(x)/dx^2 = 0$   
 936 and, when increasing  $W$ ,  $df(x)/dx = 0$  has, for the first time,  
 937 three roots. They are represented in Figure 3, bottom panel in the  
 938 main text.

### 939 Appendix B: Precipitation of particles with various shapes

940 The formalism associated with the homogeneous nucleation and  
 941 growth of spherical particles has been presented in the main text.  
 942 However, most solids, except amorphous ones, are non-isotropic and  
 943 their external shape, which departs from the sphere, reflects the  
 944 relative energies of their low index faces, as recognized by Wulff  
 945 (Müller and Kern, 2000 and references therein). Indeed, Wulff  
 946 theorem states that, at equilibrium, the distance from the center  
 947 of a particle to its external facets is proportional to the surface  
 948 energy of these facets. For example, according to Wulff theorem,  
 949 the aspect ratio of tetragonal particles (basal dimensions  $l \times l$   
 950 and thickness  $e$ , Figure 12), is given by the ratio between the  
 951 surface energies of the basal and lateral faces ( $\sigma_{bas}$  and  $\sigma_{lat}$ ,  
 952 respectively):

$$\frac{e}{l} = \frac{\sigma_{bas}}{\sigma_{lat}} \quad (34)$$

This result can be extended to the case of particles in equilibrium  
 with a substrate on which they lie on their

959 basal face. In this case,  $\sigma_{bas}$  is relevant for the face in 974  
 960 contact with the AS, and  $\sigma_{bas} - W_{adh}$  for the one in 975  
 961 contact with the substrate ( $W_{adh}$  the adhesion energy). 976  
 962 Their aspect ratio is then given by the Wulff-Kaishev 977  
 963 theorem:

$$\frac{e}{l} = \frac{\sigma_{bas} - W_{adh}/2}{\sigma_{lat}} \quad (35)$$

964 If, instead of the basal face, one of the lateral faces 981  
 965 is in contact with the substrate, their equilibrium shape  
 966 involves three inequivalent dimensions  $l$ ,  $l'$  et  $e$ . The ratio 982  
 967 between these lengths is then equal to:

$$\frac{e}{\sigma_{bas}} = \frac{l}{\sigma_{lat}} = \frac{l'}{\sigma_{lat} - W_{adh}/2} \quad (36)$$

968 The corresponding expression for rhombohedral parti- 986  
 969 cles lying on a substrate on their basal face is:

$$\frac{e}{l} = \sqrt{3} \frac{\sigma_{bas} - W_{adh}/2}{\sigma_{lat}} \quad (37)$$

970 Similar reasoning can be done for other particle shapes.

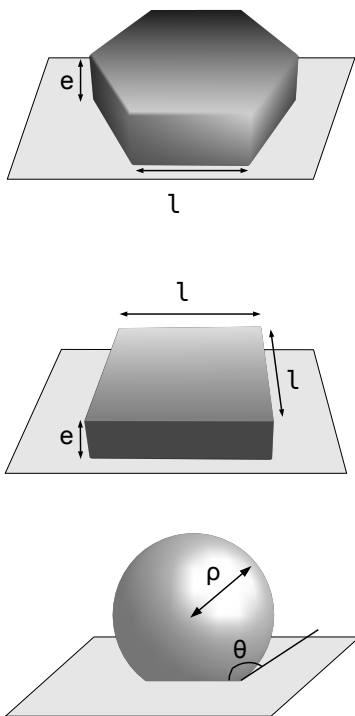


FIG. 12: Representation of rhombohedral, tetragonal and spherical cap particle shapes (from top to bottom).

971 With these elements in mind, one can consider homo- 1012  
 972 geneous as well as heterogeneous nucleation of particles, 1013  
 973 assumed to have the Wulff (homogeneous nucleation) 1014

Wulff-Kaishev (heterogeneous nucleation) shapes (Müller and Kern, 2000). The generalized expression of the change in Gibbs free energy for the formation of a critical nucleus then reads:

$$\Delta G(n, x) = -nk_B T \ln I(x) + n^{2/3} v(x)^{2/3} X \bar{\sigma} \quad (38)$$

The geometric factor  $X$  and the average surface energy  $\bar{\sigma}$  have the following expressions for simple nucleus shapes and for homogeneous or heterogeneous nucleation (Fritz et al., 2009):

- spherical particles:

$$X = (36\pi\Phi(\theta))^{1/3} ; \bar{\sigma} = \sigma \quad (39)$$

$\theta$  is the wetting angle with the substrate, given by the Young-Dupré equation  $-\sigma \cos \theta = \sigma - W_{adh}$ , and  $\Phi(\theta) = (1 - \cos \theta)^2 (2 + \cos \theta) / 4$ . For a strong adhesion to the substrate, the wetting angle is equal to  $0^\circ$ , and it is equal to  $180^\circ$  when no wetting occurs (which is also the case for homogeneous nucleation).

- tetragonal particles lying on their basal face:

$$X = 6 ; \bar{\sigma} = (\sigma_{lat}^2 (\sigma_{bas} - W_{adh}/2))^{1/3} \quad (40)$$

- tetragonal particles lying on their lateral face:

$$X = 6 ; \bar{\sigma} = (\sigma_{lat} \sigma_{bas} (\sigma_{lat} - W_{adh}/2))^{1/3} \quad (41)$$

- hexagonal particles lying on their basal face:

$$X = 36^{1/3} \sqrt{3} ; \bar{\sigma} = (\sigma_{lat}^2 (\sigma_{bas} - W_{adh}/2))^{1/3} \quad (42)$$

993 To obtain the time evolution of all dimensions during  
 994 growth, one assumes that the particles keep their equilib-  
 995 rium shape, which allows the use of equations similar to  
 996 20 and 22 of the main text for one dimension, deduction  
 997 of the others from the relationships written above for the  
 998 ratios between  $e$ ,  $l$  and  $l'$ , and estimation of the volume  
 999  $V$  of the particle and finally the number of formula units  
 1000  $n = V/v$ .

### 1001 Appendix C: Precipitation of a SS with compo- 1002 sition dependent surface energy

1003 This appendix specifies the modifications to introduce  
 1004 in the formalism which describes SS precipitation when  
 1005 their surface energy depends on composition. The main  
 1006 difference from the simplified treatment, presented in the  
 1007 main text, comes from the existence of surface enrich-  
 1008 ment effects  $n_{ACs}$  and  $n_{BCs}$  of AC and BC composition.  
 1009 Starting from a reference state in which the nuclei have  
 1010 a sharp boundary with the aqueous solution (Gibbs divid-  
 1011 ing surface), such surface excess quantities have to be  
 introduced, so that the Gibbs adsorption equation can be  
 fulfilled (Adamson, 1960; Laaksonen et al., 1999; Noppel  
 et al., 2002; Gaman et al., 2005).

1015 The change in Gibbs free energy  $\Delta G(n, x)$  for nucle-1050  
1016 ation now reads:

$$\Delta G(n, x) = -nk_B T \ln I(x) + n^{2/3} v(x)^{2/3} X \overline{\sigma(x)} - n_{BCs} k_B T \ln\left(\frac{I_{BC}}{x \lambda_{BC}(x)}\right) - n_{ACs} k_B T \ln\left(\frac{I_{AC}}{(1-x) \lambda_{AC}(x)}\right) \quad (43)$$

1017 The  $X$  parameter and the average surface energy  $\overline{\sigma(x)}$   
1018 have been defined in Appendix B for particles of various  
1019 shapes. Here  $\overline{\sigma}$  is explicitly a function of  $x$ . The two last  
1020 terms in Eq. 43 involve surface excess quantities  $n_{ACs}$   
1021 and  $n_{BCs}$ , multiplied by the corresponding changes in  
1022 chemical potential  $\Delta\mu_{AC}$  and  $\Delta\mu_{BC}$ . The surface ex-  
1023 cesses are algebraic quantities, which can take positive  
1024 as well as negative values.

1025 The expression of the critical nuclei size  $n_m(x)$ , ob-  
1026 tained from the maximum of  $\Delta G(n, x)$  with respect to  
1027  $x$  is the same as in Equation 13. In order to obtain the  
1028 critical nucleus composition, via the maximum of the nu-  
1029 cleation rate, the derivative of  $\Delta G_m(x)$  with respect to  
1030  $x$  has to be performed, with  $\Delta G_m(x) = \Delta G(n_m(x), x)$   
1031 equal to:

$$\frac{\Delta G_m(x)}{k_B T} = \frac{u(x)}{\ln^2 I(x)} - n_{BCs} k_B T \ln\left(\frac{I_{BC}}{x \lambda_{BC}(x)}\right) - n_{ACs} k_B T \ln\left(\frac{I_{AC}}{(1-x) \lambda_{AC}(x)}\right) \quad (44)$$

1032 and  $u(x)$  given in Equation 13. The part which de-  
1033 pends on  $d\overline{\sigma(x)}/dx$  and the excess quantities  $n_{ACs}$  and  
1034  $n_{BCs}$  vanishes, because it represents the Gibbs adsorp-  
1035 tion isotherm equation (Adamson, 1960):

$$n(x)^{2/3} v(x)^{2/3} X \frac{d\overline{\sigma(x)}}{dx} = -n_{ACs} \frac{d\Delta\mu_{AC}}{dx} - n_{BCs} \frac{d\Delta\mu_{BC}}{dx} \quad (45)$$

1036 A particularly simple choice for the Gibbs dividing sur-  
1037 face is that for which the surface energy does not de-  
1038 pend upon the curvature of the surface, in which case  
1039 the surface excesses fulfill the relationship  $n_{ACs} v_{AC} +$   
1040  $n_{BCs} v_{BC} = 0$  (Laaksonen et al., 1999). Associated with  
1041 Eq. 45, it leads to the following values of  $n_{ACs}$  and  $n_{BCs}$ :

$$n_{ACs}(x) = \frac{n(x)^{2/3} X x (1-x) v_{BC}}{k_B T v(x)^{1/3} [1-2x(1-x)\{A_0 + A_1(6x-3)\}]} * \frac{d\overline{\sigma(x)}}{dx} \quad (46)$$

$$n_{BCs}(x) = -\frac{n(x)^{2/3} X x (1-x) v_{AC}}{k_B T v(x)^{1/3} [1-2x(1-x)\{A_0 + A_1(6x-3)\}]} * \frac{d\overline{\sigma(x)}}{dx}$$

1042 They depend on  $x$  and are proportional to the critical  
1043 nucleus area, while  $n(x)$  is proportional to the nucleus  
1044 volume. They vanish if the surface energy is composition  
1045 independent. In the absence of detailed information on  
1046 the  $x$  dependence of  $\sigma(x)$ , a linear law may be assumed  
1047 between the end-member values of  $\sigma$ .

1048 Excess quantities also contribute to the variation of  
1049 Gibbs free energy during growth. The energetic cost to

change the dimensions of a particle  $\delta\Delta G(x)$  reads:

$$\delta\Delta G(x) = -\frac{\delta V}{v(x)} k_B T \ln I(x) + \delta E_s - \delta n_{BCs} k_B T \ln\left(\frac{I_{BC}}{x \lambda_{BC}(x)}\right) - \delta n_{ACs} k_B T \ln\left(\frac{I_{AC}}{(1-x) \lambda_{AC}(x)}\right) \quad (47)$$

It is related to its change of volume  $\delta V$ , its change of  
total surface energy  $\delta E_s$  (now a function of  $x$  through  
 $\overline{\sigma(x)}$ ), and its change in excess surface quantities  $\delta n_{ACs}$   
and  $\delta n_{BCs}$ . In the minimization of  $\delta\Delta G(x)$ , the part  
which depends on  $d\overline{\sigma(x)}/dx$  and the excess quantities  
 $\delta n_{ACs}$  and  $\delta n_{BCs}$  is formally similar to that written for  
nucleation, and yields similar expressions for  $\delta n_{ACs}$  and  
 $\delta n_{BCs}$  (Equation 46).

Finally, excess quantities have to be taken into account  
in the feed-back equations (M=AC or BC):

$$q_M(t) = \int_0^t F(t_1) (n^*(t_1) - 1) X_M(t_1) dt_1 + \int_0^t F(t_1) dt_1 \int_{t_1}^t dt_3 \frac{dn(t_1, t_3)}{dt_3} X_M(t_3) + \int_0^t F(t_1) n_{Ms}(t_1) dt_1 \quad (48)$$

#### Appendix D: Composition of the critical nuclei

The methodology to determine the composition  $x^*$  of  
the critical nucleus is very similar to that used to find the  
composition  $x_{st}$  of the SS at stoichiometric saturation  
(Appendix A). Indeed,  $x^*$  is obtained from the minimum  
of the nucleation barrier  $\Delta G_m(x)$ :

$$\frac{\Delta G_m(x)}{k_B T} = \frac{u(x)}{\ln^2 I(x)} \propto \left(\frac{v(x)}{\ln I(x)}\right)^2 \quad (49)$$

In the right hand side of this equality, we have evidenced  
the terms which depend on  $x$ . Minimizing  $\Delta G_m(x)$  with  
respect to  $x$  thus amounts to minimizing  $-\ln I(x)/v(x)$ .

By comparison with Appendix A, it first appears ob-  
vious that the composition  $x^*$  of the critical nucleus is  
equal to  $x_{st}$  when the formula unit volume  $v(x)$  of the  
SS is independent on  $x$ , because then only the minimiza-  
tion of  $-\ln I(x)$  must be found. Moreover, we note that  
the minimum of  $-\ln I(x)/v(x)$  coincides with that of  
the function  $g(x)$  equal to:

$$g(x) = -\frac{\ln I(x)}{v(x)} + \frac{\ln I_{AC}}{v_{AC}} \quad (50)$$

$g(x)$  can also be written:

$$v(x)g(x) = x \ln x + (1-x) \ln(1-x) + x(1-x)[A_0 + A_1(2x-1)] - x \ln W' \quad (51)$$

Aside from the parameters  $A_0$  and  $A_1$ , it depends on  
the ratio  $z = v_{BC}/v_{AC}$  of the end-member formula unit

volumes ( $v(x) = v_{AC}[1 - x + zx]$ ) and on the composition of the aqueous solution, which enters in a compact way via the ratio  $W' = I_{BC}/I_{AC}^z$ .

The derivative of  $g(x)$  is such that:

$$\frac{v(x)^2}{v_{AC}} \frac{dg(x)}{dx} = \ln x - z \ln(1-x) - \ln W' + A_0 [(1-x)^2 - zx^2] + A_1 [4x^3(1-z) + 3x^2(z-3) + 6x - 1] \quad (52)$$

The terms which depend on  $A_0$  and  $A_1$  turn out to be equal to  $\ln \lambda_{BC} - z \ln \lambda_{AC}$ , so that equating  $dg(x)/dx$  to zero leads to the implicit equation which determines  $x^*$  (Equation 16 in the main text):

$$\left( \frac{I_{AC}}{(1-x^*)\lambda_{AC}(x^*)} \right)^{v_{BC}} = \left( \frac{I_{BC}}{x^*\lambda_{BC}(x^*)} \right)^{v_{AC}} \quad (53)$$

The composition  $x^*$  of the critical nucleus is thus obtained when simultaneously  $dg(x)/dx = 0$  and  $g(x)$  is minimal. The discussion proceeds along steps similar to those relevant for  $x_{st}$ . Depending upon the regions of parameter space  $\{A_0, A_1\}$  (which now depends on  $z$ ),  $g(x)$  may be a convex function with a single minimum. Alternatively, it may display one minimum, or two minima and a maximum, depending upon the value of  $W'$ . When the latter case occurs, the composition of the critical nuclei is equal to the root  $x$  which corresponds to the lowest value of  $g(x)$ .

### Appendix E: Conditions of occurrence of the various scenarios of precipitation

In this appendix, we derive formal relationships allowing the determination of  $dW'/dt$ , a crucial quantity to assess which scenario will take place. Moreover, we specify the relative percentage of each phase when phase separation takes place in Scenario #4.

We recast the feed-back equation under the following form:

$$\begin{aligned} \frac{d[A]}{dt} &= -D_0(t)(1-x^*(t)) + D_A(t) \\ \frac{d[B]}{dt} &= -D_0(t)x^*(t) + D_B(t) \\ \frac{d[C]}{dt} &= -D_0(t) + D_C(t) \end{aligned} \quad (54)$$

In these expressions,  $D_0(t)$  represents the time derivative of the number of formula units withdrawn from the AS with composition  $x^*$ , while  $D_A(t)$ ,  $D_B(t)$  and  $D_C(t)$  are the variations of A, B and C activities due to either particle redissolution (thus with a surface composition different from  $x^*(t)$ ) or dissolution/precipitation of other minerals present in the AS.

The time derivative  $\ln W'$  reads:

$$\frac{1}{W'} \frac{dW'}{dt} = \frac{1}{[B]} \frac{d[B]}{dt} - \frac{z}{[A]} \frac{d[A]}{dt} + \frac{(1-z)}{[C]} \frac{d[C]}{dt} \quad (55)$$

which, after some algebra and using Eq. 54, may be recast under the following form:

$$\frac{1}{W'} \frac{dW'}{dt} = W'' - D_0(t) \left( \frac{x^*(t)}{[B]} - \frac{z(1-x^*(t))}{[A]} \right) \quad (56)$$

with:

$$W'' = \frac{D_B}{[B]} - \frac{zD_A}{[A]} + \frac{(1-z)D_C}{[C]} - D_0(t) \frac{(1-z)}{[C]} \quad (57)$$

We have separated the contribution  $W''$  to  $dW'/dt$  which does not present a discontinuity, from the one (second term on the right hand side of Eq. 56) which does present a discontinuity, due to the jump of  $x^*(t)$  between  $x_1$  and  $x_2$ . In Eqs. 54, 56 and 57, all terms relative to  $[C]$  have to be skipped when precipitation of bimetallic  $A_{1-x}B_x$  particles is considered.

Whenever Scenario #4 takes place, the cancellation of  $dW'/dt$  when  $W' = W_c$  yields the relative amounts  $D_0(t)\alpha$  and  $D_0(t)(1-\alpha)$  of the two SSs with composition  $x_1$  and  $x_2$  when phase separation occurs. From Eq. 56, one obtains:

$$\begin{aligned} \frac{1}{W'} \frac{dW'}{dt} = 0 = & W'' - D_0(t)\alpha \left( \frac{x_1}{[B]} - \frac{z(1-x_1)}{[A]} \right) \\ & - D_0(t)(1-\alpha) \left( \frac{x_2}{[B]} - \frac{z(1-x_2)}{[A]} \right) \end{aligned} \quad (58)$$

and thus:

$$\alpha = \frac{W'' - D_0(t) \left( \frac{x_2}{[B]} - \frac{z(1-x_2)}{[A]} \right)}{D_0(t)(x_1 - x_2) \left[ \frac{1}{[B]} + \frac{z}{[A]} \right]} \quad (59)$$

All these expressions may be easily evaluated numerically to assess which is the scenario relevant for the case under study and, in the case where Scenario #4 applies, Eq. 59 gives the extent of phase separation and its time dependence.

In particular, under the assumptions made in Sections VIB and VII,  $dW'/dt$  takes the simplified form:

$$\frac{1}{W'} \frac{dW'}{dt} \propto \left( \frac{x^*(t)}{[B]} - \frac{z(1-x^*(t))}{[A]} \right) \quad (60)$$

which allows the slope discontinuity between  $W' < W'_c$  and  $W' > W'_c$  to be evaluated by replacing  $x^*$  by  $x_1$  or  $x_2$ , respectively. Moreover, under the same assumptions, when phase separation takes place, the relative percentages  $\alpha$  and  $(1-\alpha)$  of the two SSs with composition  $x_1$  and  $x_2$  are given by:

$$\alpha = - \frac{(x_2 - (1-x_2) \frac{K_{BC}}{K_{AC}})}{(1-2x_2) \left( 1 + \frac{K_{BC}}{K_{AC}} \right)} \quad (61)$$

and are independent of time.

## IX. REFERENCES

- 1146  
1147 Adamson, A.W., 1960. Physical chemistry of surfaces. Interscience Publishers.  
1148  
1149 Astilleros, J.M., Pina, C.M., Fernández-Díaz, L., Putnis, A., 2003. Nanoscale growth of solids crystallising from multicomponent aqueous solutions. *Surface Science* 545, L767-L773.  
1150  
1151  
1152  
1153 Astilleros, J.M., Pina, C.M., Fernández-Díaz, L., Prieto, M., Putnis, A., 2006. Nanoscale phenomena during the growth of solid solutions on calcite 1014 surfaces. *Chemical Geology* 225, 322-335.  
1154  
1155  
1156  
1157 Aziz, M.J., 1988. Non-equilibrium interface kinetics during rapid solidification: theory and experiment. *Mater. Sci. Eng.* 98, 369-372.  
1158  
1159  
1160 Baronne, A., 1982. Ostwald ripening in solution. The case of calcite and mica. *Estudios Geol.* 38, 185-198.  
1161  
1162 Benisek, A., Dachs, E., 2012. A relationship to estimate the excess entropy of mixing; Application in silicate solid solutions and binary alloys. *J. of Alloys and Compounds* 527, 127-131.  
1163  
1164  
1165  
1166 Blanc, Ph., Lassin, A., Piantone, P., Azaroual, M., Jacquemet, N., Fabbri, A., Gaucher, E.C., 2012. Thermomodem: A geochemical database focused on low temperature water/rock interactions and waste materials. *Applied Geochemistry* Vol. 27, Issue 10, 2107-2116.  
1167  
1168  
1169  
1170  
1171 Börjesson, S., Emren, A., Ekberg, C., 1997. A thermodynamic model for the calcium silicate hydrate gel modelled as non-ideal binary solid solutions. *Cement and Concrete Research* Vol. 27, N° 11, 1649-1657.  
1172  
1173  
1174  
1175 Brandt, F., Curti, E., Klinkenberg, M., Rozov, K., Bosbach, D., 2015. Replacement of barite by (Ba,Ra)SO<sub>4</sub> solid solution at close-to-equilibrium conditions: A combined experimental and theoretical study. *Geochimica et Cosmochim. Acta* 155, 1-15.  
1176  
1177  
1178  
1179  
1180 Burton, W.K., Cabrera, N., Frank, F., 1951. The growth of crystals and the equilibrium structure of their surfaces. *Philos Trans R Soc* 243, 299-358.  
1181  
1182  
1183 Casey, W.H., Chai, L., Navrotsky, A., Rock, P.A., 1996. Thermochemistry of mixing strontianite [SrCO<sub>3</sub>(s)] and aragonite [CaCO<sub>3</sub>(s)] to form Ca<sub>x</sub>Sr<sub>1-x</sub>(CO<sub>3</sub>)(s) solid solutions. *Geochim. Cosmochim. Acta* 60, 933-940.  
1184  
1185  
1186  
1187  
1188 Chai, L., Navrotsky, A., 1996. Synthesis, characterization, and enthalpy of mixing of the (Fe,Mg)CO<sub>3</sub> solid solution. *Geochim. Cosmochim. Acta* 60, 4377-4383.  
1189  
1190  
1191 Crocket, J.H., Winchester, J.W., 1966. Coprecipitation of zinc with calcium carbonate. *Geochim. et Cosmochim. Acta.* 30, 1093-1109.  
1192  
1193  
1194 Doerner, H.A., Hoskins, W.M., 1925. Coprecipitation of radium and barium sulfates. *J. Amer. Chem. Soc.* 47, 662-675.  
1195  
1196  
1197 Drever, J.I., 1984. *The Chemistry of Weathering*. Reidel Publishing Co. 324p.  
1198  
1199 Fernández-González, A., Andara, A., Alía, J.M., Prieto, M., 2006. Miscibility in the CaSO<sub>4</sub>.2H<sub>2</sub>O-CaSeO<sub>4</sub>.2H<sub>2</sub>O system: Implications for the crystallisation and dehydration behaviour. *Chem. Geol.* 225, 256-265.  
1200  
1201  
1202  
1203  
1204  
1205  
1206  
1207  
1208  
1209  
1210  
1211  
1212  
1213  
1214  
1215  
1216  
1217  
1218  
1219  
1220  
1221  
1222  
1223  
1224  
1225  
1226  
1227  
1228  
1229  
1230  
1231  
1232  
1233  
1234  
1235  
1236  
1237  
1238  
1239  
1240  
1241  
1242  
1243  
1244  
1245  
1246  
1247  
1248  
1249  
1250  
1251  
1252  
1253  
1254  
1255  
1256  
1257  
1258  
1259  
1260  
1261  
1262  
1263  
1264  
1265  
1266  
1267  
1268  
1269  
1270  
1271  
1272  
1273  
1274  
1275  
1276  
1277  
1278  
1279  
1280  
1281  
1282  
1283  
1284  
1285  
1286  
1287  
1288  
1289  
1290  
1291  
1292  
1293  
1294  
1295  
1296  
1297  
1298  
1299  
1300  
1301  
1302  
1303  
1304  
1305  
1306  
1307  
1308  
1309  
1310  
1311  
1312  
1313  
1314  
1315  
1316  
1317  
1318  
1319  
1320  
1321  
1322  
1323  
1324  
1325  
1326  
1327  
1328  
1329  
1330  
1331  
1332  
1333  
1334  
1335  
1336  
1337  
1338  
1339  
1340  
1341  
1342  
1343  
1344  
1345  
1346  
1347  
1348  
1349  
1350  
1351  
1352  
1353  
1354  
1355  
1356  
1357  
1358  
1359  
1360  
1361  
1362  
1363  
1364  
1365  
1366  
1367  
1368  
1369  
1370  
1371  
1372  
1373  
1374  
1375  
1376  
1377  
1378  
1379  
1380  
1381  
1382  
1383  
1384  
1385  
1386  
1387  
1388  
1389  
1390  
1391  
1392  
1393  
1394  
1395  
1396  
1397  
1398  
1399  
1400  
1401  
1402  
1403  
1404  
1405  
1406  
1407  
1408  
1409  
1410  
1411  
1412  
1413  
1414  
1415  
1416  
1417  
1418  
1419  
1420  
1421  
1422  
1423  
1424  
1425  
1426  
1427  
1428  
1429  
1430  
1431  
1432  
1433  
1434  
1435  
1436  
1437  
1438  
1439  
1440  
1441  
1442  
1443  
1444  
1445  
1446  
1447  
1448  
1449  
1450  
1451  
1452  
1453  
1454  
1455  
1456  
1457  
1458  
1459  
1460  
1461  
1462  
1463  
1464  
1465  
1466  
1467  
1468  
1469  
1470  
1471  
1472  
1473  
1474  
1475  
1476  
1477  
1478  
1479  
1480  
1481  
1482  
1483  
1484  
1485  
1486  
1487  
1488  
1489  
1490  
1491  
1492  
1493  
1494  
1495  
1496  
1497  
1498  
1499  
1500  
1501  
1502  
1503  
1504  
1505  
1506  
1507  
1508  
1509  
1510  
1511  
1512  
1513  
1514  
1515  
1516  
1517  
1518  
1519  
1520  
1521  
1522  
1523  
1524  
1525  
1526  
1527  
1528  
1529  
1530  
1531  
1532  
1533  
1534  
1535  
1536  
1537  
1538  
1539  
1540  
1541  
1542  
1543  
1544  
1545  
1546  
1547  
1548  
1549  
1550  
1551  
1552  
1553  
1554  
1555  
1556  
1557  
1558  
1559  
1560  
1561  
1562  
1563  
1564  
1565  
1566  
1567  
1568  
1569  
1570  
1571  
1572  
1573  
1574  
1575  
1576  
1577  
1578  
1579  
1580  
1581  
1582  
1583  
1584  
1585  
1586  
1587  
1588  
1589  
1590  
1591  
1592  
1593  
1594  
1595  
1596  
1597  
1598  
1599  
1600  
1601  
1602  
1603  
1604  
1605  
1606  
1607  
1608  
1609  
1610  
1611  
1612  
1613  
1614  
1615  
1616  
1617  
1618  
1619  
1620  
1621  
1622  
1623  
1624  
1625  
1626  
1627  
1628  
1629  
1630  
1631  
1632  
1633  
1634  
1635  
1636  
1637  
1638  
1639  
1640  
1641  
1642  
1643  
1644  
1645  
1646  
1647  
1648  
1649  
1650  
1651  
1652  
1653  
1654  
1655  
1656  
1657  
1658  
1659  
1660  
1661  
1662  
1663  
1664  
1665  
1666  
1667  
1668  
1669  
1670  
1671  
1672  
1673  
1674  
1675  
1676  
1677  
1678  
1679  
1680  
1681  
1682  
1683  
1684  
1685  
1686  
1687  
1688  
1689  
1690  
1691  
1692  
1693  
1694  
1695  
1696  
1697  
1698  
1699  
1700  
1701  
1702  
1703  
1704  
1705  
1706  
1707  
1708  
1709  
1710  
1711  
1712  
1713  
1714  
1715  
1716  
1717  
1718  
1719  
1720  
1721  
1722  
1723  
1724  
1725  
1726  
1727  
1728  
1729  
1730  
1731  
1732  
1733  
1734  
1735  
1736  
1737  
1738  
1739  
1740  
1741  
1742  
1743  
1744  
1745  
1746  
1747  
1748  
1749  
1750  
1751  
1752  
1753  
1754  
1755  
1756  
1757  
1758  
1759  
1760  
1761  
1762  
1763  
1764  
1765  
1766  
1767  
1768  
1769  
1770  
1771  
1772  
1773  
1774  
1775  
1776  
1777  
1778  
1779  
1780  
1781  
1782  
1783  
1784  
1785  
1786  
1787  
1788  
1789  
1790  
1791  
1792  
1793  
1794  
1795  
1796  
1797  
1798  
1799  
1800  
1801  
1802  
1803  
1804  
1805  
1806  
1807  
1808  
1809  
1810  
1811  
1812  
1813  
1814  
1815  
1816  
1817  
1818  
1819  
1820  
1821  
1822  
1823  
1824  
1825  
1826  
1827  
1828  
1829  
1830  
1831  
1832  
1833  
1834  
1835  
1836  
1837  
1838  
1839  
1840  
1841  
1842  
1843  
1844  
1845  
1846  
1847  
1848  
1849  
1850  
1851  
1852  
1853  
1854  
1855  
1856  
1857  
1858  
1859  
1860  
1861  
1862  
1863  
1864  
1865  
1866  
1867  
1868  
1869  
1870  
1871  
1872  
1873  
1874  
1875  
1876  
1877  
1878  
1879  
1880  
1881  
1882  
1883  
1884  
1885  
1886  
1887  
1888  
1889  
1890  
1891  
1892  
1893  
1894  
1895  
1896  
1897  
1898  
1899  
1900  
1901  
1902  
1903  
1904  
1905  
1906  
1907  
1908  
1909  
1910  
1911  
1912  
1913  
1914  
1915  
1916  
1917  
1918  
1919  
1920  
1921  
1922  
1923  
1924  
1925  
1926  
1927  
1928  
1929  
1930  
1931  
1932  
1933  
1934  
1935  
1936  
1937  
1938  
1939  
1940  
1941  
1942  
1943  
1944  
1945  
1946  
1947  
1948  
1949  
1950  
1951  
1952  
1953  
1954  
1955  
1956  
1957  
1958  
1959  
1960  
1961  
1962  
1963  
1964  
1965  
1966  
1967  
1968  
1969  
1970  
1971  
1972  
1973  
1974  
1975  
1976  
1977  
1978  
1979  
1980  
1981  
1982  
1983  
1984  
1985  
1986  
1987  
1988  
1989  
1990  
1991  
1992  
1993  
1994  
1995  
1996  
1997  
1998  
1999  
2000  
2001  
2002  
2003  
2004  
2005  
2006  
2007  
2008  
2009  
2010  
2011  
2012  
2013  
2014  
2015  
2016  
2017  
2018  
2019  
2020  
2021  
2022  
2023  
2024  
2025  
2026  
2027  
2028  
2029  
2030  
2031  
2032  
2033  
2034  
2035  
2036  
2037  
2038  
2039  
2040  
2041  
2042  
2043  
2044  
2045  
2046  
2047  
2048  
2049  
2050  
2051  
2052  
2053  
2054  
2055  
2056  
2057  
2058  
2059  
2060  
2061  
2062  
2063  
2064  
2065  
2066  
2067  
2068  
2069  
2070  
2071  
2072  
2073  
2074  
2075  
2076  
2077  
2078  
2079  
2080  
2081  
2082  
2083  
2084  
2085  
2086  
2087  
2088  
2089  
2090  
2091  
2092  
2093  
2094  
2095  
2096  
2097  
2098  
2099  
2100  
2101  
2102  
2103  
2104  
2105  
2106  
2107  
2108  
2109  
2110  
2111  
2112  
2113  
2114  
2115  
2116  
2117  
2118  
2119  
2120  
2121  
2122  
2123  
2124  
2125  
2126  
2127  
2128  
2129  
2130  
2131  
2132  
2133  
2134  
2135  
2136  
2137  
2138  
2139  
2140  
2141  
2142  
2143  
2144  
2145  
2146  
2147  
2148  
2149  
2150  
2151  
2152  
2153  
2154  
2155  
2156  
2157  
2158  
2159  
2160  
2161  
2162  
2163  
2164  
2165  
2166  
2167  
2168  
2169  
2170  
2171  
2172  
2173  
2174  
2175  
2176  
2177  
2178  
2179  
2180  
2181  
2182  
2183  
2184  
2185  
2186  
2187  
2188  
2189  
2190  
2191  
2192  
2193  
2194  
2195  
2196  
2197  
2198  
2199  
2200  
2201  
2202  
2203  
2204  
2205  
2206  
2207  
2208  
2209  
2210  
2211  
2212  
2213  
2214  
2215  
2216  
2217  
2218  
2219  
2220  
2221  
2222  
2223  
2224  
2225  
2226  
2227  
2228  
2229  
2230  
2231  
2232  
2233  
2234  
2235  
2236  
2237  
2238  
2239  
2240  
2241  
2242  
2243  
2244  
2245  
2246  
2247  
2248  
2249  
2250  
2251  
2252  
2253  
2254  
2255  
2256  
2257  
2258  
2259  
2260  
2261  
2262  
2263  
2264  
2265  
2266  
2267  
2268  
2269  
2270  
2271  
2272  
2273  
2274  
2275  
2276  
2277  
2278  
2279  
2280  
2281  
2282  
2283  
2284  
2285  
2286  
2287  
2288  
2289  
2290  
2291  
2292  
2293  
2294  
2295  
2296  
2297  
2298  
2299  
2300  
2301  
2302  
2303  
2304  
2305  
2306  
2307  
2308  
2309  
2310  
2311  
2312  
2313  
2314  
2315  
2316  
2317  
2318  
2319  
2320  
2321  
2322  
2323  
2324  
2325  
2326  
2327  
2328  
2329  
2330  
2331  
2332  
2333  
2334  
2335  
2336  
2337  
2338  
2339  
2340  
2341  
2342  
2343  
2344  
2345  
2346  
2347  
2348  
2349  
2350  
2351  
2352  
2353  
2354  
2355  
2356  
2357  
2358  
2359  
2360  
2361  
2362  
2363  
2364  
2365  
2366  
2367  
2368  
2369  
2370  
2371  
2372  
2373  
2374  
2375  
2376  
2377  
2378  
2379  
2380  
2381  
2382  
2383  
2384  
2385  
2386  
2387  
2388  
2389  
2390  
2391  
2392  
2393  
2394  
2395  
2396  
2397  
2398  
2399  
2400  
2401  
2402  
2403  
2404  
2405  
2406  
2407  
2408  
2409  
2410  
2411  
2412  
2413  
2414  
2415  
2416  
2417  
2418  
2419  
2420  
2421  
2422  
2423  
2424  
2425  
2426  
2427  
2428  
2429  
2430  
2431  
2432  
2433  
2434  
2435  
2436  
2437  
2438  
2439  
2440  
2441  
2442  
2443  
2444  
2445  
2446  
2447  
2448  
2449  
2450  
2451  
2452  
2453  
2454  
2455  
2456  
2457  
2458  
2459  
2460  
2461  
2462  
2463  
2464  
2465  
2466  
2467  
2468  
2469  
2470  
2471  
2472  
2473  
2474  
2475  
2476  
2477  
2478  
2479  
2480  
2481  
2482  
2483  
2484  
2485  
2486  
2487  
2488  
2489  
2490  
2491  
2492  
2493  
2494  
2495  
2496  
2497  
2498  
2499  
2500  
2501  
2502  
2503  
2504  
2505  
2506  
2507  
2508  
2509  
2510  
2511  
2512  
2513  
2514  
2515  
2516  
2517  
2518  
2519  
2520  
2521  
2522  
2523  
2524  
2525  
2526  
2527  
2528  
2529  
2530  
2531  
2532  
2533  
2534  
2535  
2536  
2537  
2538  
2539  
2540  
2541  
2542  
2543  
2544  
2545  
2546  
2547  
2548  
2549  
2550  
2551  
2552  
2553  
2554  
2555  
2556  
2557  
2558  
2559  
2560  
2561  
2562  
2563  
2564  
2565  
2566  
2567  
2568  
2569  
2570  
2571  
2572  
2573  
2574  
2575  
2576  
2577  
2578  
2579  
2580  
2581  
2582  
2583  
2584  
2585  
2586  
2587  
2588  
2589  
2590  
2591  
2592  
2593  
2594  
2595  
2596  
2597  
2598  
2599  
2600  
2601  
2602  
2603  
2604  
2605  
2606  
2607  
2608  
2609  
2610  
2611  
2612  
2613  
2614  
2615  
2616  
2617  
2618  
2619  
2620  
2621  
2622  
2623  
2624  
2625  
2626  
2627  
2628  
2629  
2630  
2631  
2632  
2633  
2634  
2635  
2636  
2637  
2638  
2639  
2640  
2641  
2642  
2643  
2644  
2645  
2646  
2647  
2648  
2649  
2650  
2651  
2652  
2653  
2654  
2655  
2656  
2657  
2658  
2659  
2660  
2661  
2662  
2663  
2664  
2665  
2666  
2667  
2668  
2669  
2670  
2671  
2672  
2673  
2674  
2675  
2676  
2677  
2678  
2679  
2680  
2681  
2682  
2683  
2684  
2685  
2686  
2687  
2688  
2689  
2690  
2691  
2692  
2693  
2694  
2695  
2696  
2697  
2698  
2699  
2700  
2701  
2702  
2703  
2704  
2705  
2706  
2707  
2708  
2709  
2710  
2711  
2712  
2713  
2714  
2715  
2716  
2717  
2718  
2719  
2720  
2721  
2722  
2723  
2724  
2725  
2726  
2727  
2728  
2729  
2730  
2731  
2732  
2733  
2734  
2735  
2736  
2737  
2738  
2739  
2740  
2741  
2742  
2743  
2744  
2745  
2746  
2747  
2748  
2749  
2750  
2751  
2752  
2753  
2754  
2755  
2756  
2757  
2758  
2759  
2760  
2761  
2762  
2763  
2764  
2765  
2766  
2767  
2768  
2769  
2770  
2771  
2772  
2773  
2774  
2775  
2776  
2777  
2778  
2779  
2780  
2781  
2782  
2783  
2784  
2785  
2786  
2787  
2788  
2789  
2790  
2791  
2792  
2793  
2794  
2795  
2796  
2797  
2798  
2799  
2800  
2801  
2802  
2803  
2804  
2805  
2806  
2807  
2808  
2809  
2810  
2811  
2812  
2813  
2814  
2815  
2816  
2817  
2818  
2819  
2820  
2821  
2822  
2823  
2824  
2825  
2826  
2827  
2828  
2829  
2830  
2831  
2832  
2833  
2834  
2835  
2836  
2837  
2838  
2839  
2840  
2841  
2842  
2843  
2844  
2845  
2846  
2847  
2848  
2849  
2850  
2851  
2852  
2853  
2854  
2855  
2856  
2857  
2858  
2859  
2860  
2861  
2862  
2863  
2864  
2865  
2866  
2867  
2868  
2869  
2870  
2871  
2872  
2873  
2874  
2875  
2876  
2877  
2878  
2879  
2880  
2881  
2882  
2883  
2884  
2885  
2886  
2887  
2888  
2889  
2890  
2891  
2892  
2893  
2894  
2895  
2896  
2897  
2898  
2899  
2900  
2901  
2902  
2903  
2904  
2905  
2906  
2907  
2908  
2909  
2910  
2911  
2912  
2913  
2914  
2915  
2916  
2917  
2918  
2919  
2920  
2921  
2922  
2923  
2924  
2925  
2926  
2927  
2928  
2929  
2930  
2931  
2932  
2933  
2934  
2935  
2936  
2937  
2938  
2939  
2940  
2941  
2942  
2943  
2944  
2945  
2946  
2947  
2948  
2949  
2950  
2951  
2952  
2953  
2954  
2955  
2956  
2957  
2958  
2959  
2960  
2961  
2962  
2963  
2964  
2965  
2966  
2967  
2968  
2969  
2970  
2971  
2972  
2973  
2974  
2975  
2976  
2977  
2978  
2979  
2980  
2981  
2982  
2983  
2984  
2985  
2986  
2987  
2988  
2989  
2990  
2991  
2992  
2993  
2994  
2995  
2996  
2997  
2998  
2999  
3000

- Lippmann, F., 1980. Phase diagrams depicting the aqueous solubility of binary mineral systems. *N. Jahrb. Mineral. Abh.* 139, 1-25.
- Lippmann, F., 1982. Stable and metastable solubility diagrams for the system  $\text{CaCO}_3\text{-MgCO}_3\text{-H}_2\text{O}$  at ordinary temperature. *Bull. Mineral.* 105, 273-279.
- Lyapunov, A.M., 1992. *The General Problem of the Stability of Motion* (A. T. Fuller translation.) Taylor & Francis, London.
- Madé, B., Clément, A., Fritz, B., 1994. Modelling mineral/solution interactions : the thermodynamic and kinetic code KINDISP. *Comp. Geosci.* 20 (9), 1347-163.
- Major, K.J., De, C., Obare, S.O., 2009. Recent Advances in the Synthesis of Plasmonic Bimetallic Nanoparticles. *Plasmonics* 4, 61-78.
- Markov, I.V., 1995. *Crystal growth for Beginners fundamentals of nucleation, crystal growth and epitaxy* World Scientific (Singapore, New Jersey, London, Hong Kong).
- Matsumoto, N., Kitamura, M., 2001. Effective distribution coefficients of a binary ideal solid solution controlled by kink kinetics. *J. of Crystal Growth* 222, 667-676.
- Matsumoto, K., Irisawa, T., Kitamura, M., Yokoyama, E., Kumagai, Y., Kouhkitu, A., 2005. Effective distribution of an ideal solid solution crystal : Monte Carlo simulation. *J. of Crystal Growth* 276, 635-642.
- Meunier, A., Velde, B., 1989. Solid solutions in illite/semctite mixed layer minerals and illite. *Amer. Mineralogist* 74, 1106-1112.
- Millot, G., 1970. *Geology of Clays*. Translated from french. Springer-Verlag, 425p.
- Müller, P., Kern, R., 2000. Equilibrium nanoshape changes induced by epitaxial stress (generalized Wulff-Kaishef theorem). *Surf. Sci.* 457, 229-253.
- Mullin, J.W., 1993. *Crystallization*. (Butterworth-Heinemann).
- Noguera, C., Fritz, B., Clément, A., Baronnet, A., 2006a. Nucleation, growth and ageing in closed systems I : a unified model for precipitation in solution, condensation in vapor phase and crystallization in the melt. *J. of Crystal Growth* 297, 180-186.
- Noguera, C., Fritz, B., Clément, A., Baronnet, A., 2006b. Nucleation, growth and ageing in closed systems II : dynamics of formation of a new phase. *J. of Crystal Growth* 297, 187-198.
- Noguera, C., Fritz, B., Clément, A., Amal, Y., 2010. Simulation of the nucleation and growth of binary solid solutions in aqueous solutions. *Chem Geol.* 269, 89-99.
- Noguera, C., Fritz, B., Clément, A., 2012. A Theoretical Treatment of the Precipitation of Doubly Substituted Solid Solutions in Aqueous Solutions. *Cryst. Growth & Des.* 12, 3444-3457.
- Noppel, M., Vehkamäki, H., Kulmala, M., 2002. An improved model for hydrate formation in sulfuric acid-water nucleation. *J. Chem. Phys.* 116, 218-228.
- Nourtier-Mazauric, E., Guy, B., Fritz, B., Brosse, E., Garcia, D., Clément, A., 2005. Modeling the dissolution/precipitation of ideal solid solutions. *Oil Gas Sci. Technol. Re. IFP* 60, 401-415.
- Ostwald, W.Z., 1900. *Phys. Chem. Stoichiometrie. Verwandsch* 34, 495.
- Parbhakar, K., Lewandowski, J., Dao, L.H., 1995. Simulation model for Ostwald ripening in liquids. *J. Colloid Interf. Sci.* 174, 142-147.
- Parkhurst, D.L., Appelo, C.A.J., 1999. User's guide to PHREEQC (version 2). A computer program for speciation, batch-reaction, one-dimensional transport, and inverse geochemical calculations. US Geological Survey Water-Resources Investigations Report 99-4259 (312 pp.).
- Peng, Z., Yang, H., 2009. Designer platinum nanoparticles: Control of shape, composition in alloy, nanostructure and electrocatalytic property. *Nano Today* 4, 143-164.
- Pina, C.M., Enders, M., Putnis, A., 2000. The composition of solid solutions crystallising from aqueous solutions: The influence of supersaturation and growth mechanisms. *Chem. Geol.* 168, 195-210.
- Pina, C.M., Putnis, A., 2002. The kinetics of nucleation of solid solutions from aqueous solutions: A new model for calculating non-equilibrium distribution coefficients. *Geochim. et Cosmochim. Acta* Vol. 66, No. 2, 185-192.
- Prieto, M., Putnis, A., Fernández-Díaz, L., 1993. Crystallization of solid solutions from aqueous solutions in a porous medium: zoning in  $(\text{Ba,Sr})\text{SO}_4$ . *Geol. Mag.* 130, 289.
- Prieto, M., Fernández-Gonzalez, A., Putnis, A., Fernández-Díaz, L., 1997. Nucleation, growth, and zoning phenomena in crystallizing  $(\text{Ba,Sr})\text{CO}_3$ ,  $\text{Ba}(\text{SO}_4,\text{CrO}_4)$ ,  $(\text{Ba,Sr})\text{SO}_4$ , and  $(\text{Cd,Ca})\text{CO}_3$  solid solutions from aqueous solutions. *Geochim. et Cosmochim. Acta* Vol. 61, No. 16, 3383-3397.
- Prieto, M., 2009. Thermodynamics of Solid Solution-Aqueous Solution. In : *Thermodynamics and Kinetics of Water-Rock Interaction. Reviews in Mineralogy and Geochemistry* vol. 70, 47-85. Mineralogical Society of America and Geochemical Society (Eds).
- Putnis, A., Pina, C.M., Astilleros, J.M., Fernández-Díaz, L., Prieto, M., 2002. Nucleation of solid solutions crystallizing from aqueous solutions. *Phil. Trans. R. Soc. Lond. A* 361, 615-632.
- Reiss, H., Shugard, M., 1976. On the composition of nuclei in binary systems. *J. Chem. Phys.* 65, 5280-5293.
- Rhada, A.V., Navrotsky, A., 2013. Thermodynamics of Carbonates, *Reviews in Mineralogy and Geochemistry* 77, 73-121.
- Roozeboom, H.W.B., 1904. *Die Heterogenen Gleichgewichte vom Standpunkte der Phasenlehre II*. Friedrich Vieweg und Sohn, Braunschweig.
- Sánchez-Pastor, N., Pina, C.M., Fernández-Díaz, L., 2006. Relationships between crystal morphology and composition in the  $(\text{Ba,Sr})\text{SO}_4\text{-H}_2\text{O}$  solid solution-aqueous solution system. *Chem. Geol.* 225, 266-277.
- Shtukenberg, A.G., Punin, Y.O., Azimov, P.Y., 2010.

- 1375 Crystallization in Solid Solution-Aqueous Solution Sys<sup>1383</sup>  
1376 tems: Thermodynamic and Kinetic Approaches. Crys<sup>1384</sup>  
1377 tallography Reports Vol. 55, No. 2, 328-341. <sup>1385</sup>
- 1378 Vinograd, V.L., Brandt, F., Rozov, K., Klinkenberg<sup>1386</sup>  
1379 M., Refson, K., Winkler, B., Bosbach, D., 2013. Solid<sup>1387</sup>  
1380 aqueous equilibrium in the BaSO<sub>4</sub>-RaSO<sub>4</sub>-H<sub>2</sub>O system<sup>1388</sup>  
1381 first principles calculation and a thermodynamic assess<sup>1389</sup>  
1382 ment. Geochim. et Cosmochim. Acta 122, 398-417. <sup>1390</sup>
- Walker, C.S., Savage, D., Tyrer, M., Ragnarsdottir,  
K.V., 2007. Non-ideal solid solution modeling for syn-  
thetic calcium silicate hydrate. Cement and Concrete  
Research 37, 502-511.
- Zhang, H., Okuni, J., Toshima, N., 2011. One-pot syn-  
thesis of Ag-Au bimetallic nanoparticles with Au shell  
and their high catalytic activity for aerobic glucose oxi-  
dation. J. Colloids and Interf. Sci. 354, 131-138.
-

## LIST OF SYMBOLS

## Latin characters

$A_0, A_1$	First and second coefficients of the Guggenheim expansion (dimensionless)
$[A]$	Activity of the aqueous species A
$D_0$	Time derivative of the number of formula units withdrawn from the AS with composition $x^*$
$D_A, D_B, D_C$	Contributions to the time derivative of [A], [B] or [C] which are continuous at $W'_c$
$E_s$	Total surface energy (J)
$F(x)$	Nucleation frequency (number of nuclei/s/liter of solution)
$F_0$	Prefactor of the nucleation frequency (number of nuclei/s/liter of solution)
$\Delta G_M$	Standard changes in Gibbs free energy for the dissolution of the M end-member (M=AC or BC)
$\Delta G(x)$	Change of Gibbs free energy for a SS of composition $x$ during precipitation or growth
$\Delta G_M^E(x)$	Excess change of Gibbs free energy of mixing for a SS of composition $x$
$\Delta G(n, x)$	Change in Gibbs free energy for the formation of a nucleus containing $n$ formula units of composition $x$
$\Delta G_m(x)$	maximum of $\Delta G(n, x)$ with respect to $n$
$\Delta H_M(x)$	Enthalpy of mixing for a SS of composition $x$
$I_M$	Saturation state of the AS with respect to the pure end-member M (M=AC or BC)
$I(x)$	Stoichiometric saturation state of the AS with respect to a SS of composition $x$
$I_c(x^*)$	Critical saturation state of the AS with respect to a SS of composition $x$
$k_B$	Boltzmann constant ( $1.3806504 \times 10^{-23}$ J/K)
$K_M$	Solubility product of the end-member M (M=AC or BC)
$K(x)$	Stoichiometric solubility product of a SS of composition $x$
$l(t_1, t)$	Lateral length at time $t$ of a rhomboedral or a tetragonal particle created at time $t_1$ (m)
$n_m(x)$	Number of growth units in a particle of composition $x$ at the maximum of $\Delta G(n, x)$ with respect to $n$
$n(t_1, t)$	Number of growth units at time $t$ in a particle created at time $t_1$
$n_M(x)$	Surface excess quantities of end-member M in a particle
$Q(x)$	Ionic activity product of a SS of composition $x$
$q_M(t)$	Amount of end-member M withdrawn at time $t$ from the AS (formula unit/liter of solution)
$R$	Gaz constant (8.314472 J/K/mol)
$T$	Temperature (K)
$x_0$	Composition of a SS at thermodynamic equilibrium with an AS
$x_{st}$	Composition of a SS at stoichiometric saturation with an AS
$x^*$	Critical nucleus composition
$x_1, x_2$	Values of the SS composition at the limit of the discontinuity in strongly non-ideal SSs
$\bar{x}$	Mean composition value of the SS when phase separation occurs
$v_M$	Volume of one formula unit of end-member M ( $m^3$ )
$v(x)$	Volume of one formula unit of a SS of composition $x$ ( $m^3$ )
$W$	Ratio of the saturation states of the pure end-members $W = I_{BC}/I_{AC}$
$W_c$	Critical value of $W$ at the composition discontinuity
$W'$	$W' = I_{BC}/(I_{AC})^z$
$W'_c$	Critical value of $W'$ at the composition discontinuity
$dW'_1/dt, dW'_2/dt$	Slopes of $dW'/dt$ on the left and right of the discontinuity, respectively
$W''$	Contribution to $dW'/dt$ which is continuous at $W'_c$
$W_{adh}$	Adhesion energy, in the case of heterogeneous nucleation (J/m <sup>2</sup> )
$X$	Geometric factor entering the total surface energy of the particles
$z$	Ratio of end-members formula unit volumes $z = v_{BC}/v_{AC}$

## Greek characters

$\alpha$	Percentage of the two SSs of composition $x_1$ and $x_2$ when phase separation occurs
$\Delta\mu_M$	Change in chemical potential of one formula unit of the M end-member during precipitation (M=AC or BC)
$\kappa$	Linear growth constant (m/s)
$\lambda_M$	Activity coefficient of the end-member M in the SS (M=AC or BC)
$\rho(t_1, t)$	Radius at time $t$ of a spherical particle created at time $t_1$ (m)
$\sigma(x)$	Mean surface energy per unit area of SS particles of composition $x$ (J/m <sup>2</sup> )
$\sigma_{lat}, \sigma_{bas}$	Lateral and basal surface energies per unit area of non-spherical particles (J/m <sup>2</sup> )
$\theta$	Wetting angle